



OPEN ACCESS

EDITED BY
Manuel Will,
University of Tübingen, Germany

REVIEWED BY
Erich Fisher,
University of Algarve, Portugal
Ingrid Ward,
University of Western Australia, Australia

*CORRESPONDENCE
Sarah Wurz,
sarah.wurz@wits.ac.za

SPECIALTY SECTION
This article was submitted to Quaternary
Science, Geomorphology and
Paleoenvironment,
a section of the journal
Frontiers in Earth Science

RECEIVED 23 July 2022
ACCEPTED 07 October 2022
PUBLISHED 07 November 2022

CITATION
Wurz S, Pickering R and Mentzer SM
(2022), U-Th dating, taphonomy, and
taxonomy of shell middens at Klasies
River main site indicate stable and
systematic coastal exploitation by
MIS 5c-d.
Front. Earth Sci. 10:1001370.
doi: 10.3389/feart.2022.1001370

COPYRIGHT
© 2022 Wurz, Pickering and Mentzer.
This is an open-access article
distributed under the terms of the
[Creative Commons Attribution License
\(CC BY\)](https://creativecommons.org/licenses/by/4.0/). The use, distribution or
reproduction in other forums is
permitted, provided the original
author(s) and the copyright owner(s) are
credited and that the original
publication in this journal is cited, in
accordance with accepted academic
practice. No use, distribution or
reproduction is permitted which does
not comply with these terms.

U-Th dating, taphonomy, and taxonomy of shell middens at Klasies River main site indicate stable and systematic coastal exploitation by MIS 5c-d

Sarah Wurz^{1,2*}, Robyn Pickering³ and Susan M. Mentzer^{4,5}

¹School of Geography, Archaeology and Environmental Studies, University of the Witwatersrand, Johannesburg, South Africa, ²Centre for Early Sapience Behaviour, University of Bergen, Bergen, Norway, ³Department of Geological Sciences, University of Cape Town, Cape Town, South Africa, ⁴Senckenberg Centre for Human Evolution and Palaeoenvironment (S-HEP), University of Tübingen, Tübingen, Germany, ⁵Institute for Archaeological Sciences, Department of Geosciences, University of Tübingen, Tübingen, Germany

The archaeological record, particularly of shellfish, from the Klasies River main site (KRM) is important in understanding the fluctuating nature of coastal occupational patterns and changing coastal ecologies. In this paper, we provide new uranium–thorium (U–Th) dates for one of the earlier phases of coastal exploitation at KRM, and the microstratigraphic analyses generate novel information about the taphonomy of shell-bearing deposits from the Later Stone Age (LSA) to the MSA I period that, in turn, provide a broader context for middening at the site. A wide range of syndepositional taphonomic processes related to human activities and post-depositional effects include burning, fragmentation and compaction, chemical alteration, and cementation. Despite such issues influencing recovery, shellfish data are informative and are presented from three layers of the Witness Baulk: Shell Midden One (SMONE), Black Occupational Soils (BOS), and Silty Black Soils (SBLS). These coarse shell midden deposits exhibit visible decalcification coupled with cementation with secondary carbonate formation in association with conditions of high moisture and soft sedimentation deformation of the underlying sediments of SBLS. This stratigraphy section is chronologically anchored for the first time using U–Th dating of speleothems associated with a hiatus after the deposition of BOS. The three ages, $110,060 \pm 1,100$, $109,800 \pm 970$, and $106,000 \pm 2,100$ years, place the BOS layer as the base of the SASL sub-member at over 110 ka, making the underlying middens from the LBS member even older. The zooarchaeological analyses of the three layers indicate coastal ecological changes from more sheltered conditions prior to the hiatus, with the exploitation of alikreukel and brown mussels predominating. Before 110 ka, in BOS and SBLS, more exposed coastal conditions occurred, and the diversity of exploited shellfish increased. SMONE and BOS are associated with MSA II/Mossel Bay lower lithic technology and SBLS with MSA I technology, indicating asynchronous coastal ecological and technological changes. The MIS 5c-d evidence for early coastal occupation at KRM provides details on the period during which coastal occupation became stable and systematic on the

South African coast and puts the KRM amongst the handful of sites with shell-bearing deposits, occurring prior to 110 ka in South Africa.

KEYWORDS

Klasies River, shell midden analysis, micromorphology analysis, U-Th ages, coastal exploitation

1 Introduction

Coastal archaeological sites with shell middens that reflect regular, intentional, and systematic exploitation of coastal resources such as shellfish, fish, birds, and other terrestrial resources through hunting, gathering, and scavenging provide evidence for coastal adaptation in various degrees (Jerardino, 2016a; Will et al., 2016, 2019). Shell middens are inferred when occupational debris is shell supported, and the shell thus dominates the matrix as shell middens would have formed quickly with deposition rates of shell exceeding that of sediments (Marean, 2014). Some researchers prefer the term “shell matrix sites,” which include shell middens, shell mounds, and shell-bearing deposits, all composed of at least 50% shells (Andersen, 2000; Villagran, 2019). Within the Cape region of South Africa (Figure 1), most of the shell middens relate to the later Middle Stone Age (MSA) dating back to 100,000 years ago (ka) (Klein and Bird, 2016; Will et al., 2016, 2019) and the Later Stone Age (LSA), with rich Holocene data from the West Coast. The Holocene data document the complexity and variability of coastal occupational patterns and present an ideal opportunity for theoretical developments (Jerardino, 2016a). Although studies on MSA coastal adaptation from the Cape feature prominently in the research landscape, especially in relation to modern human origins, only a few MSA shell middens occur before 100 ka (Tribolo et al., 2022). The exploitation of marine resources at early MSA coastal sites has been linked to socio-biological evolutionary advances for *Homo sapiens*. It has, for example, been theorized that the fatty acids from shellfish provided significant nutritional benefits to early modern human populations on the coast (Parkington et al., 2010; Kyriacou et al., 2016) and that the Cape coastal sites demonstrate the first instance, 110 ka, of the exploitation of dense predictable resources (Marean, 2016).

A key aspect of research into the relationship between early modern humans and their adaptation to coastal living and the level to which their lifestyles depended on these marine resources has been the identification of the earliest incidences of coastal resource exploitation. At Pinnacle Point Cave 13B (PP 13B), optically stimulated luminescence (OSL) ages of ca. 164 ka indicate the earliest evidence for shellfish collection on the South African coast and globally (Jacobs, 2010; Jerardino and Marean, 2010; Marean, 2010, 2016). It has been suggested that coastal occupation occurred between 130 and 115 ka on the Cape West Coast (Will et al., 2013; Kyriacou et al., 2015), and this is

supported by recent chronologies. Ysterfontein 1 (YFT 1) (Figure 1) shell-bearing deposits (Klein et al., 2004; Avery et al., 2008) have been dated to between 119.9 and 113.1 ka using $^{230}\text{Th}/\text{U}$ burial dating on ostrich eggshells (Niespolo et al., 2021a). At Hoedjies Punt 1 (HDP 1), situated close to YFT 1, OSL dating yielded ages of between ~130 and 100 ka (Tribolo et al., 2022) for layers with shellfish (Kyriacou et al., 2015). It seems that a strong signal for organized and systematic exploitation of coastal resources emerged only from around 100 ka in the southern Cape, at sites such as Blombos Cave (BBC), Klasies River main site (KRM) (Henshilwood et al., 2001; Will et al., 2016, 2019; Brenner et al., 2022), and Pinnacle Point 13B (Jerardino and Marean 2010). However, earlier systematic coastal foraging may have taken place, but the evidence has been largely eroded away (Fisher et al., 2010; Marean et al., 2010).

A key and long-studied site with shell middens is KRM (Figure 1). This site provides an ideal opportunity to investigate *Homo sapiens* coastal exploitation on the southern Cape coast as it was made home by many generations of hunter-fisher-gatherers, from early MIS 5 into MIS 3, and again in the LSA (Singer and Wymer, 1982; Deacon, 1995; Wurz et al., 2018). The lowermost MSA I and MSA II/Mossel Bay layers at KRM are broadly dated to between 80 and ca 115 ka, with very few dates that can be directly associated with the deposits themselves. Moreover, interest is growing in detailed microscopic studies on formation processes and taphonomy in middening (Oertle et al., 2022), a perspective that is key to understanding coastal exploitation. The aim of this paper is thus threefold: to report new dates for a section of the earliest MSA II/Mossel Bay shell-bearing deposits, to provide new information on the taphonomy of the middens and other shell-bearing deposits through the sequence by means of micromorphological analysis, and to report on the analysis of the shellfish from the most recently excavated middens from KRM.

KRM is currently situated within the Greater Cape Floristic Region within the Fynbos biome (Allsopp et al., 2014) and, presently, the vegetation is characterized by a mixture of thicket, forest, grass, and fynbos (van Wijk et al., 2017). The nearby Tsitsikamma mountain's southern slopes receive an average of 875–1,375 mm rainfall per year, and at Storms River, 25 km west from KRM, 810 mm is received (van Wijk et al., 2017). KRM falls within the year-round rainfall zone (YRZ) close to its eastern boundary (Chase & Meadows 2007). In the YRZ, precipitation is determined by the South Atlantic Anticyclone system, which frequently leads to stratiform

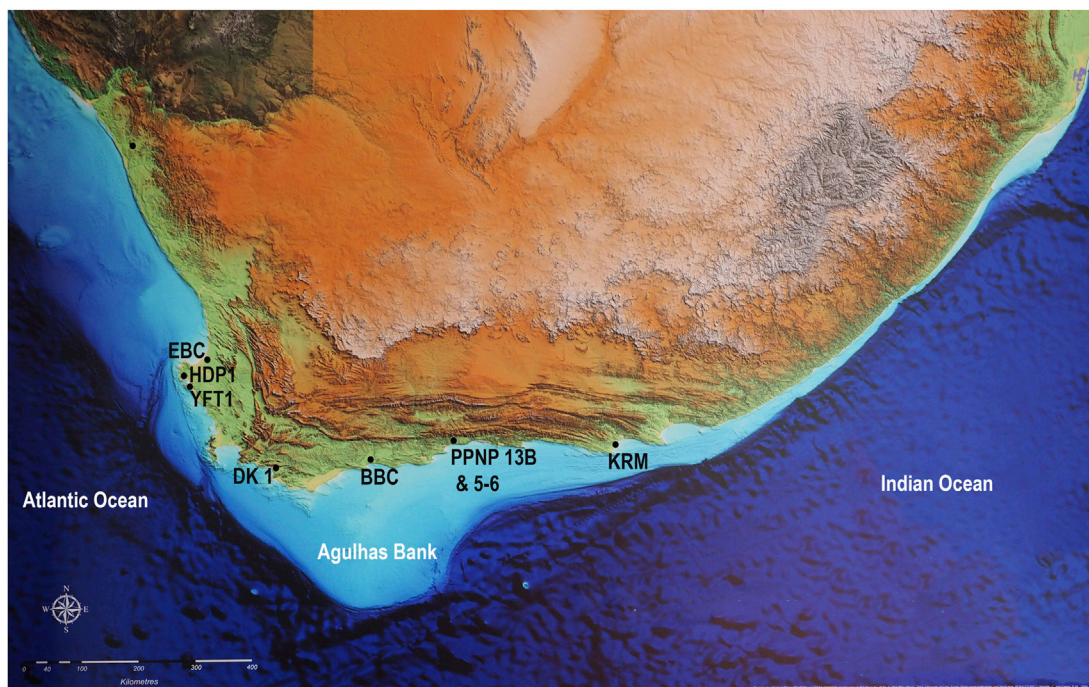


FIGURE 1

Map with sites with shell midden deposits discussed in the text: Elands Bay Cave (EBC), Hoedjies Punt 1 (HDP1), Ysterfontein 1 (YFT1), Die Kelders (DK1), Blombos Cave (BBC), Pinnacle Point sites 13B and 5–6 (PP 13B & 5-6), and Klasies River Main site (KRM).

rainfall in the winter months and tropical temperate troughs that form convective rain, mostly in summer (Engelbrecht et al., 2015; Braun et al., 2017).

The narrowness of the Palaeo-Agulhas Plain and the steep topography of the coastline along the south east coast (de Wet and Compton 2021) (Figure 1) suggest that the shore was in close proximity to KRM during many time periods of relatively lower sea levels during the Late Pleistocene (Van Andel 1989; Langejans et al., 2017). KRM is thus a suitable location to investigate coastal adaptation because it was frequently near the coast. The presence of MSA shell middens at KRM has been known for a long time (Voigt, 1973a, b; Singer and Wymer, 1982; Thackeray, 1988; Klein et al., 2004); however, the current dating framework for especially the earlier deposits provides an overlapping array of age determinations (Niespolo et al., 2021b; Morrissey et al., 2022). Furthermore, many middens are impacted by post-depositional processes that result in poor recovery of the identifiable shell during excavation.

The KRM site consists of a group of two caves formed in quartzite, Cave 1 and Cave 1C, one large recess, Cave 2, and two cliff-face rock-shelters, 1A and 1B (termed “caves” hereafter), which collectively preserve around 21 m of MSA and LSA deposits. KRM was excavated in three cycles, in the 1960s (Singer and Wymer, 1982), in the period between 1984 and 1995 (Deacon, 1995), and most recently, since 2015 (Wurz et al.,

2018). Singer and Wymer recognized several large-scale layers occurring across the different areas of the main site. These were incorporated in Deacon’s more detailed lithostratigraphic system that consists of members (Figure 2), comprising many small-scale excavation units (Morrissey et al., 2022). The earliest layers occur in Cave 1 and Cave 1B, and occupational debris might have built up continuously in the Caves, but the possible connection was lost due to erosion (Morrissey et al., 2022).

Singer and Wymer excavated large areas of Cave 1 but left a Witness Baulk. The LBS, SAS Lower, and SAS Upper sub-members in Cave 1 contain *in situ* deposits, and the SAS Wedge (SASW) and SAS Rubble (SASR) sub-members relate to *ex situ* material that accumulated when primary occupation took place against the cliff face of Cave 1A. A 1.5 X 1.5 area at the southern end of the Witness Baulk was excavated by Deacon and subsequently by Wurz. The LBS and parts of the SAS member in cave 1/1A also occur in Square AA43, where Cave 1A and Cave 1 intersect, but the stratigraphic relationship between this area and the Witness Baulk is uncertain (Morrissey et al., 2022). The topmost deposits of the Upper member occur only in Caves 1A and 2. The members relate to various cultural stages, with the LBS member containing MSA I lithic artifacts, the SAS associated with the MSA II or the Mossel Bay technocomplex, and the Upper member with the Howiesons Poort (HP) and post-Howiesons Poort (also known as the MSA III) cultural stages

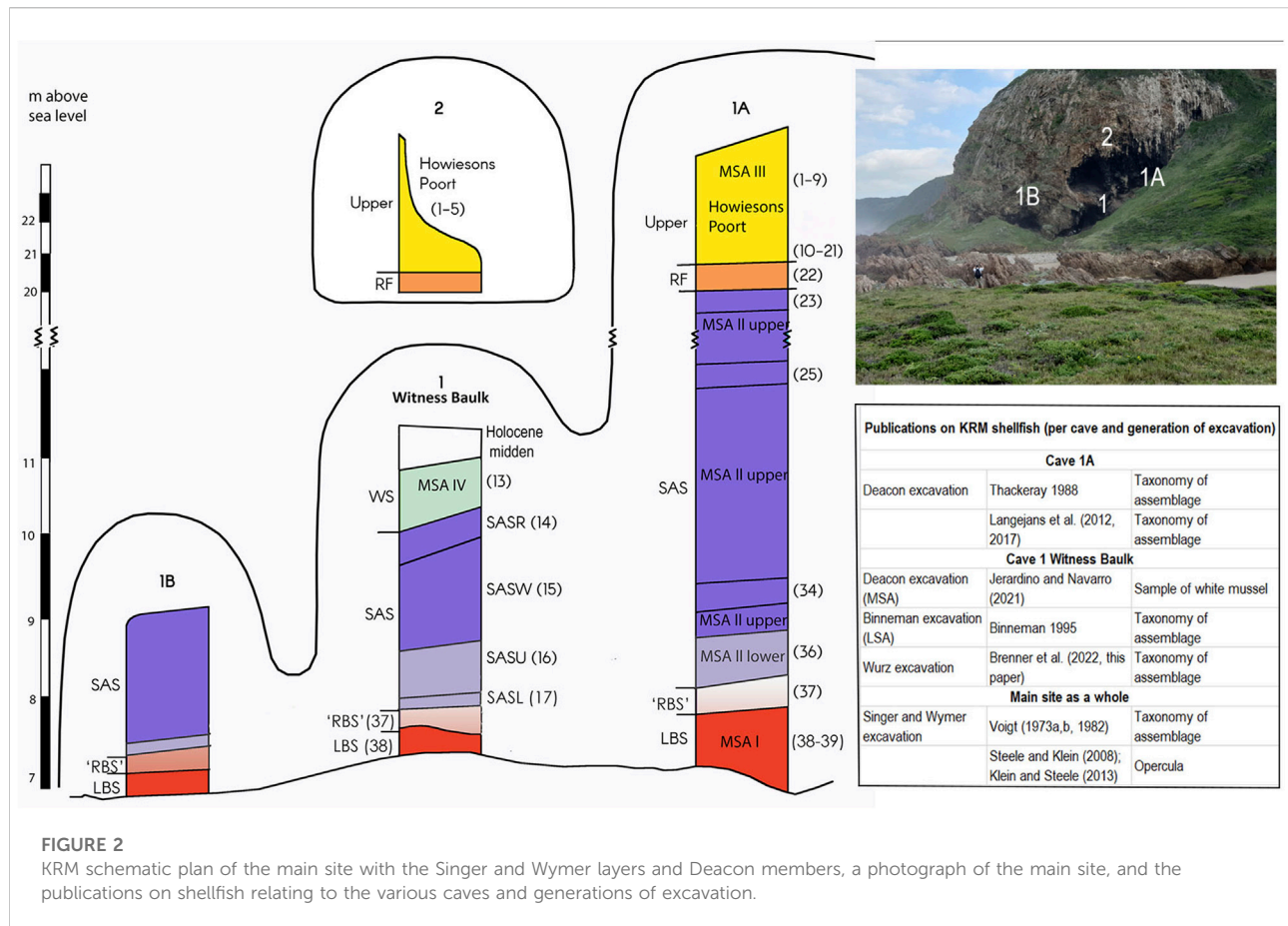


FIGURE 2 KRM schematic plan of the main site with the Singer and Wymer layers and Deacon members, a photograph of the main site, and the publications on shellfish relating to the various caves and generations of excavation.

(Singer and Wymer 1982; Deacon and Geleijnse 1988; Wurz 2002).

The deposits of the Witness Baulk in Cave 1 from MIS 5c-d [93–115 ka, see Wadley (2015) for the boundaries of the MIS stages] are the focus of this contribution, although shell middens from various parts of the site are described from a micromorphological perspective to elucidate the taphonomy and provide the broader context. The SAS member in Cave 1 is associated with MIS 5a-d. For the SASR sub-member at the top of the Witness Baulk, U-series dating of stalagmites, not connected to the deposits, yielded ages of between ca. 85–100 ka (Vogel et al., 2021). The underlying SASW sub-member is associated with an OSL age of ca. 70 ka (Feathers, 2002), and the SASU sub-member with ages of 89 ka [amino acid racemization (AAR) age, Bada and Deems (1975)] and 68 ka [OSL age using multi- and single aliquot techniques, Feathers (2002)]. A uranium–thorium (U-Th) date of ca. 126 ka on flowstone from the base of SASU in the Witness Baulk provides a maximum age for this part of the sequence. An age older than 100 ka has been suggested for the base of SASU (Wurz et al., 2018), as the SASR, Singer and Wymer's Layer 14, relates to U-series ages of 85–100 ka as mentioned above.

The age estimates that relate most closely to the SASL sub-member are from a tooth from Singer & Wymer's layer 17 (Figure 2) dated using ESR (Grün et al., 1990). Late uptake results are 93.5 ± 10.4 ka and 88.3 ± 7.8 ka for sub-samples of this tooth, whereas later combined *in situ* U-series and ESR dating of the same tooth gave an age estimate of 101 ± 12 ka (Eggins et al., 2005). The SASL sub-member is thus older than 100 ka. As Brenner et al. (2022) mentioned, dating has been undertaken for stalagmite material from an excavated unit of the SASL called BOS Three. In this study, U-Th dating of *in situ* speleothem material from this layer is reported in detail, which narrows down the age range of this layer and the SASL sub-member.

Coastal occupation involves exploiting a range of marine-related resources, but shellfish is highlighted in this study. Over the years of research at KRM, the various excavation projects reported on shellfish data (see Figure 2 for publications on shellfish for the various caves and excavation cycles at the main site). Voigt (1973) and Voigt (1982) first published on the shellfish of the layers from the whole site excavated by Singer and Wymer (1982) at a time when molluscan fauna was frequently neglected by archaeologists. The sample available was heavily selected (Voigt, 1982). However, it provided some indication of the changing shellfish species through the sequence,

especially in relation to the relative quantities of the dominant species, brown mussel (*Perna perna*) and alikreukel (*Turbo sarmaticus*). Deacon's excavation followed more modern methods and retained all the shellfish and fragments thereof; thus, the shellfish material from Cave 1A and square AA43 from Cave 1/1A (See Figure 2) provide valuable insights into subsistence and paleoenvironmental trends from MIS 3–MIS 5 (Thackeray, 1988; Langejans et al., 2012, 2017; Dusseldorp and Langejans, 2013, 2015). The shellfish from Cave 1 Witness Baulk (SASR–SASU sub-members) comprises a large MIS 5 sample and is currently under study. Jerardino and Navarro (2021) analyzed some of the white mussels (*Donax serra*) from this sample. The shellfish recorded at KRM include species such as top shells (*Oxysteles sinensis*), alikreukel (*Turbo sarmaticus*), and whelk (*Burnupena limbosa*) that reflect the Algoa marine province with its warm waters (Langejans et al., 2012). Throughout the sequence high ranked mollusc species such as alikreukel and brown mussel from the mid-intertidal zone were targeted (Voigt, 1982; Thackeray, 1988; Langejans et al., 2012), but there are changes in the collected species through time that indicate changing coastal environments fluctuating between relatively rocky and sandy coastal habitats (Langejans et al., 2017).

2 Shell middens, dating, and geoarchaeology

2.1 Dating of middens

The LSA midden at the top of the Cave 1 sequence has been previously dated using radiocarbon on shell and charcoal (Singer and Wymer, 1982; Binneman, 1995; Nami et al., 2016) and paleomagnetism (Nami et al., 2016). At KRM, the calibrated ages obtained for the LSA II on charcoal ($2,795 \pm 85$ cal yr. BP) (Singer and Wymer, 1982) agree with those obtained on the shell ($2,655 \pm 30$ cal yr. BP) (Nami et al., 2016). However, in other contexts, radiocarbon dating of shell middens can be complicated by variations in the marine reservoir effects over time and also secondary disposal activities of humans (Deo et al., 2004). Other approaches to directly date marine shells, such as U-Th measurements, remain experimental and can be plagued by low reliability (Sherwood et al., 1994). However, a breakthrough development of the U-Th technique applied to ostrich eggshell fragments, which are also discarded in middens and are less susceptible to post-depositional alteration (Niespolo et al., 2021a), is rapidly changing this picture. Dating techniques that target geogenic lenses or layers within the middens, such as OSL or paleomagnetism, have likewise also proven successful in some South African contexts, including KRM (Nami et al., 2016). However, intercomparisons of ages on other LSA middens suggest that OSL can be complicated by human disturbance (Bateman et al., 2008). Another approach tested in South African contexts is AAR, which Bateman et al. (2008) reported as

potentially applicable in settings where materials were deeply buried.

U-Th dating of geogenic and pedogenic carbonates is a reliable approach to directly date their formation (Hellstrom and Pickering, 2015). The most important consideration in archaeological contexts is how the datable carbonate layer relates to the archaeological strata of interest. When U-Th dating is applied to secondary carbonates in open-air settings, these may have formed below the ground surface some time after the deposition of the midden material. Shell middens can develop post-depositional horizonation over time, but weathering does not always follow a typical pedogenic surface-downward trajectory (Stein, 2008). Sub-surface secondary carbonates in shell middens have been observed by Aldeias and Bicho (2016), Duarte et al. (2019), and Stein et al. (2011). However, to our knowledge, these types of materials have never been directly dated. In caves, secondary carbonates can form as flowstones and speleothems from water dripping directly onto an exposed ground surface. In these contexts, the ages obtained provide information about the timing of hiatuses in the use of the middens. U-Th dating of speleothem carbonate in shell middens is not a common approach, possibly because worldwide, a vast majority of shell middens are located in open-air settings rather than caves. However, cave middens are common in certain regions, such as Southern Africa and Scotland for marine middens and the Maghreb and Vietnam for land snail middens (Gutiérrez-Zugasti et al., 2011; Taylor et al., 2011; McAdams et al., 2022). In KRM and other sites, such as those in the PP complex, speleothems form in the quartzite caves due to the presence of an overlying lithified calcareous dune complex, which saturates the percolating water in carbonate (Bar-Matthews et al., 2010).

2.2 Geoarchaeology of middens

Geoarchaeological analysis of shell middens dates back to the pioneering work of Stein (1982, 1992, 2008). Following some of the earliest applications of micromorphology to shell middens by Goldberg and Byrd (1999). The analyses that emphasize and interpret the microstratigraphy of shell middens became more widespread with the experimental, ethnoarchaeological, and archaeological work of Villagran and colleagues (Villagran et al., 2011a; Villagran et al., 2011b; Villagran, 2014; Villagran, 2019; Villagran et al., 2021). Microstratigraphic analyses of large shell middens in South America and Europe typically reveal complicated sequences of deposition related to actual middening behaviors (e.g., dumping of food wastes); *in situ* features such as cooking hearths, trampling, and phases of weathering; and geogenic deposition (Aldeias and Bicho, 2016; Duarte et al., 2019; Ward et al., 2019). Previous micromorphological analyses of shell-midden deposits in the KRM Witness Baulk reveal a similar mixed use of space in Cave 1 during the MSA I,

with two intact hearths containing evidence for multiple firing episodes—at least one associated with the cooking of tubers—on top of layers of anthropogenic debris that included both fragments of shell and bone (Larbey et al., 2019).

Studies that employ micromorphology as a tool for studying shell midden taphonomy frequently emphasize either the impacts of human activities, such as burning and trampling (Villagran et al., 2011a; Villagran, 2014), or shoreline processes, such as marine transgressions (Ward et al., 2019; Hale et al., 2021). Villagran and Poch (2014) documented the effects of the removal of the organic component of shell and freeze-thaw processes under cold, open-air conditions. In another open-air setting, Aldeias and Bicho (2016) and Duarte et al. (2019) document the dissolution of shells near the surface and in localized areas in association with organic matrix and secondary carbonate formation as pendants on shell and cementation at depth. In caves and rock-shelters, a wider range of taphonomic processes might be expected. Linstädter and Kehl (2012) reported high variability in the preservation of shells in the Ifri Oudadane coastal rock-shelter, some of which related to human activities such as trampling and burning; however, post-depositional processes such as gypsum precipitation and the presence of soluble salts were also reported. A recent study of land snail middens in two Vietnamese caves documented some unique diagenetic processes, such as phosphatic alteration of bones in the midden, formation of secondary phosphate minerals and carbonate cement, and alteration of the shell to secondary carbonate (McAdams et al., 2022).

In South African caves and rock-shelters, similar processes have been observed impacting shell-rich deposits. At Die Kelders, for example, Goldberg (2000) documented spatially constrained dissolution of carbonates that impacted a layer that, elsewhere within the cave, was rich in both marine molluscs and land snails. In intermediate zones, he observed shell fragments undergoing decalcification and attributed the dissolution to water saturation of the sediment just above the bedrock floor of the cave. This model is similar to the basal weathering by groundwater proposed for an open-air midden by Stein (2008). Decalcification was also observed in certain layers of PP 5–6 (Karkanas et al., 2015), and in the Waterfall Bluff rock-shelter, shell dissolution was especially pronounced under the dripline (Oertle et al., 2022).

Another process observed in cave middens is the phosphatization of calcareous materials and bone. Goldberg (2000) and McAdams et al. (2022) attributed phosphatization to the possible presence of guano in the studied caves, an interpretation consistent with other studies of diagenesis in archaeological caves inhabited by bats and birds (Karkanas et al., 2000). At Elands Bay Cave—a site known for its LSA shell midden—secondary phosphatization significantly impacted the preservation of the MSA deposits such that bones and shells were completely dissolved (Miller et al., 2016). The diagenesis there is attributed to water that entered the back of the shelter

after first passing through a series of rock ledges on which birds and rock hyrax lived.

Although shell dissolution and secondary phosphatization may be enhanced in middens deposited in caves and rock-shelters, comparative micromorphological analyses of MSA age open-air middens in South Africa are exceptionally limited. One thesis conducted on the open-air site of Hoedjies Punt found the presence of phosphatic grains that may have an anthropogenic origin related to the accumulation of organic material in a mixed occupation horizon (Göden 2014). A similar anthropogenic source for secondary phosphates in Brazilian open-air shell mounds was proposed by Corrêa et al. (2013) and Villagran (2019).

At KRM, diagenetic processes impacting shells and other carbonates have been previously documented in Caves 1 and 2. Deacon (1995) reported on the differential preservation of the shell of the brown mussel, which he attributed to the major differences in the nature of the LBS middens relative to the LSA middens in Cave 1. Butzer (1982) noted that shells in Wymer's layer 37 and base 17 were partially decalcified. Deacon and Geleijnse (1988) also described load structures and soft sediment deformation in this part of the sequence (Figure 3). In Cave 2, Deacon and Geleijnse (1988) and Feathers (2002) described the significant post-depositional dissolution of carbonates that impacted the Upper Member deposits. Deacon and Geleijnse (1988) noted the preservation and cementation of “substantial shell lenses” in the western portion of the chamber, where speleothems are also present. However, in the eastern part of the chamber, they attributed volume loss to shell dissolution, which—along with bone—was sparse and fragmented in the area excavated by Wymer. Feathers (2002) applied OSL to quartz grains from the cutting in the eastern part of the chamber and found that this sample had the highest concentration of radioisotopes out of all samples collected from the site. He modeled the effects of rapid and slow dissolution of shells on the dose rates and age outcomes and found that the results favored a rapid (early) dissolution scenario.

Based on the published field observations, post-depositional processes, including compaction, soft-sediment deformation, and dissolution, have impacted the preservation of shell middens or shell-bearing deposits in different site areas (Table 1).

3 Materials and methods

3.1 Micromorphology and microanalysis

Several micromorphology blocks were collected from shell middens and shell-rich layers at KRM to observe variability in taphonomic processes (Table 1). In 2013 and 2015, blocks were carved from exposed profiles from the Deacon and Wymer excavations. The blocks were stabilized in the field with plaster and then transported to the University of Tübingen,

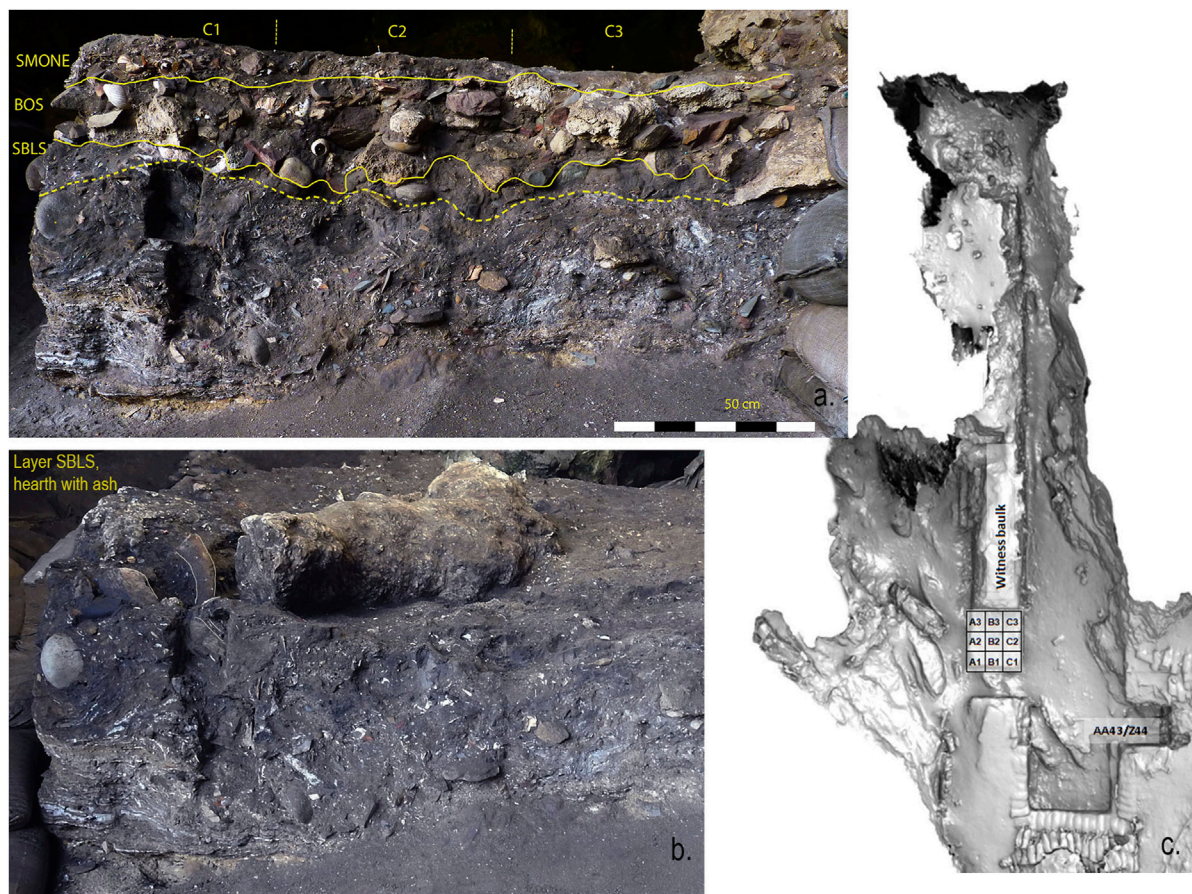


FIGURE 3

(A) East face Witness Baulk, showing the layers excavated with locations of two of the micromorphology blocks; the upper contains the very base of the SBLS. (B) Layer SBLS exposed, showing the fallen stalactite and bluebuck horncore that indicate the direction of the impact. (C) Plan of Cave 1 with Witness Baulk and excavation grid. Note that the stratigraphy presented by Wurz et al. (2018) has been revised slightly to distinguish the SBLS from the underlying deposits.

where the blocks were dried and then indurated with a mixture of polyester resin and styrene catalyzed with MEKP. After curing, the blocks were sliced, and areas were selected from the cut faces for thin-section production. In some cases, thin sections were ground thicker than the standard thickness of 30 μm due to the observed loss of the softer shell relative to the harder materials such as secondary carbonate and quartz during the grinding process. Following thin section production, the samples were scanned with a Bruker M4 Tornado micro-X-ray-fluorescence analyzer (μXRF) to yield major and trace element distribution maps. The maps were produced using dual detectors with a pixel spacing of 60 microns, a spot size of ~ 25 microns, a rhodium tube voltage of 50 kV, and a current of 600 micro-amps.

The thin sections were studied under plane- and cross-polarized light (PPL and XPL) using a petrographic microscope. Descriptive terminology followed Stoops (2003), and observations specific to shells in thin sections followed Canti (2017) and Villagran et al. (2011b), whereas fabric

analysis of shell-supported sediment followed Aldeias and Bicho (2016). Mineralogical identifications were made using optical properties, in some cases supplemented with a combination of elemental mapping and micro-Fourier transform infrared (μFTIR) spectroscopic measurements. The μFTIR measurements were made with a Cary 610 (Agilent Technologies) FTIR microscope in reflectance mode or with a germanium attenuated total reflectance accessory to yield reflectance or absorbance spectra (respectively) that were compared to an in-house digital reference library for identification purposes.

3.2 Dating

During the 2017 excavation season, several *in situ* speleothem features were encountered. These features included small stalagmites, carbonated masses, and flowstone. Lithic

TABLE 1 List of micromorphology blocks referenced in this study and their contexts, with the presence of taphonomic processes that impacted the shell.

Sample number	Site area	Stratigraphic context	Cultural context, archaeological feature	Clast-supported lenses? >50%	Heat alteration	Dissolution	Calcite cement	Phosphatization
KRM-13-01	Cave 1/ Cave 1A	SAS4 SHC, SAS4 SHB, SAS4 SH	MSA I, shell midden	×		×	×	Present, but not impacting shell
KRM-13-08	Cave 1	LBS	MSA I, shell midden, and hearths	×	×	×		Present, but not impacting shell
KRM-13-07	Cave 1	LBS	MSA I, shell midden, and hearths	×	×	×		Present, but not impacting shell
KRM-13-06	Cave 1	LBS	MSA I, shell midden, and hearths	×	×	×		Present, but not impacting shell
KRM-13-05	Cave 1	LBS, contact with SBLs	MSA I, shell midden, and hearths		×			×
KRM-15-112	Cave 1/1A	YS1B, YS1, SCB1; equivalent to SASL	MSA II, distal shell midden					
KRM-13-02	Cave 1/ Cave 1A	SAS1S, SCB2; equivalent to SBLs	MSA II			×	×	Present, but not impacting shell
KRM-13-13	Cave 1A	Upper member: CPx5, YSx3, CPx4	HP, trash midden with shell		×			
KRM-15-103	Cave 2	Upper member	HP, shell midden	×	v. Rare		×	×
KRM-15-107	Cave 2	Upper member	HP, lateral equivalent to KRM-13-103 but impacted by diagenesis			×		×
KRM-13-25	Cave 1		LSA, shell midden	×	×			

TABLE 2 U-series results.

R	Mass (g)	U Conc ± 2SE (ppb)	$^{230}\text{Th}/^{238}\text{ThA} \pm 95\% \text{ ext}$	$^{234}\text{U}/^{238}\text{UA} \pm 95\% \text{ ext}$	$^{232}\text{Th}/^{238}\text{UA} \pm 2\text{SE}$	$^{230}\text{Th}/^{232}\text{Thi} \pm 2\text{sd}$	$^{230}\text{Th}/^{232}\text{ThA}$	Age ± 2SE (years)	$[\text{}^{234}\text{U}/\text{}^{238}\text{U}]_{\text{i corr}} \pm 2\text{SE}$
5384 (KRM1, WB, A2, BOS)	0.037	655 ± 49	0.9038 ± 0.0035	1.3642 ± 0.0034	0.006287 ± 0.000045	1.50 ± 1.50	143.8	110,060 ± 1,100	1.4970 ± 0.0042
6478 (KRM1, WB, C3, BOS)	0.018	440 ± 33	0.8068 ± 0.0042	1.2498 ± 0.0034	0.014507 ± 0.000081	1.50 ± 1.50	55.6	106,000 ± 2,100	1.3369 ± 0.0045
6819 (KRM1 WB, B1, BOS)	0.032	519 ± 39	0.9275 ± 0.0037	1.4001 ± 0.0035	0.004511 ± 0.000035	1.50 ± 1.50	205.6	109,800 ± 970	1.5455 ± 0.0042

The final U-Th ages are marked in bold for emphasis.

artifacts and bone recovered from this layer also exhibited encrustations of secondary carbonate. Three of the speleothems from BOS were documented and removed for U-Th dating, one each from excavation rows A, B, and C. These samples were assigned lab numbers 5384, 6819, and 6478. Sample 5384 from square A2 is a carbonated mass. Sample 6819 from square B1 is a small stalagmite with

flowstone extending off its edges, yielding an appearance of a fried egg. Sample 6478 from square C3 is a small stalagmite of approximately 10 cm in height (Table 2).

These three speleothem samples were visually inspected and carefully cut along a vertical axis using a diamond-tipped geological saw. The flat sections were lightly polished, and the cleanest, densest carbonate layers were visually selected for

U-Th dating. A hand-held hobby drill and dentist berr was used to drill out around 1 g of powder from each chosen layer. These samples were deliberately selected to date the oldest layer of speleothem formation to provide an age estimate for the beginning of the hiatus in sedimentation. Around 300 mg of each sample was weighed out into an ultra-clean Teflon vial, spiked a mixed ^{229}Th - ^{233}U spike, calibrated against a standard HU-1 uranite solution in secular equilibrium, dissolved, and run through a standard ion-exchange chromatography set of protocols to isolate and concentrate the Th and U isotopes (Hellstrom, 2003). U and Th isotopic concentrations and ratios were then measured simultaneously using a Nu Instrument Plasma multicollector inductively coupled plasma mass spectrometer (MC-ICP-MS), again following standard measurement protocols (Hellstrom, 2003, 2006). A correction assuming an initial $^{230}\text{Th}/^{232}\text{Th}$ of 1.50 ± 1.50 was applied to all final ages to account for a detrital phase (Hellstrom, 2006).

3.3 Excavation of the SASL sub-member in the Witness Baulk and field observations

Shellfish evidence relating to coastal adaptation for three layers from the Wurz excavations of Square C1 of the Witness Baulk, Shell Midden One (SMONE), Black Occupational Soils (BOS), and Silty Black Soils (SBLs) are discussed (Figure 3). The three layers are equally well presented in square C1 (50 × 50 cm), in contrast with the rest of the Witness Baulk, where deposits from the layers occur unevenly. All tufa, speleothem material, fauna, stone, and other artifacts >20 mm were piece-plotted, and these items were not included in the calculation of the deposit volume (Table 1). The excavated deposits were first dry-sieved through 5 and 2 mm meshes. Subsequently, the coarse and fine fractions were wet sieved through very fine domestic sieves (0.5 mm), resulting in the retention of very small shell fragments, microfauna, and lithic chipping debris. The archaeological material occurs as palimpsests, and the winnowing of soils led to it being tightly stacked, often precluding the precise determination of the angle of the finds. Lithics and microfauna are plentiful, and the large mammal fauna is well preserved but frequently fragile. The marine shell is less well preserved, although it was possible to excavate a few complete shells. Land snails that occur in significant numbers (Brenner et al., 2022) are much better preserved. The lithics from SMONE–BOS relate to the MSA II lower or Mossel Bay technocomplex (Wurz, 2002; Brenner & Wurz, 2019; Wurz, 2021; Brenner et al., 2022), and a prepared core or Levallois technology was followed to produce points and some blade end products. Formal tools, when present, are mostly notched artifacts. The SBLs layer has MSA I affinities (Brenner et al., 2022), in which blade technology becomes more prominent (Wurz, 2002).

The Wurz excavation follows the Deacon stratigraphic system, and SMONE and BOS are from the SASL sub-member. Layer SMONE is equivalent to Singer and Wymer's layer 17a and BOS to layer 17b (Singer and Wymer 1982; Wurz et al., 2018). The matrix of SMONE consists of relatively loose soils and rubble with disintegrated tufa blocks, patches of leached ash and charcoal, and no *in situ* combustion features. Layer SMONE was up to 15 cm thick in square C1 but much thinner in the other squares.

The sediments from BOS, discussed in more detail in this study as it relates to the dating samples, are darker and more clayey than those of SMONE. Although the matrix is generally similar to that of SMONE with no preserved combustion features, significantly more speleothem and tufa material are present in BOS than in SMONE, and some of the lithics and anthropogenically altered fauna are covered in flowstone. A large stalactite, more than 1 m in length, fell into the BOS deposits and came to rest on SBLs, deforming them in the process. The angle of a horn core (Figure 3) captures the extent and direction of the impact. Singer and Wymer (1982) mentioned numerous blocks of soft calcite from Layer 17 excavated from other cave areas. This accords with the findings from the BOS layer, and tufa or phytokarren/photokarren may be calcite deposits that formed by biophysical/biochemical activity and dripping water (Viles, 1984; Vanara and Maire, 2006).

Due to its thickness, around 35 cm in total, BOS was excavated in arbitrary spits determined by the year of excavation (BOS One, BOS Two, and BOS Three), which assisted in investigating the site formation processes. In the top part of the layer, BOS One and BOS Two, the highest number of carnivore tooth-marked bovid specimens occurred, and more bones with transverse, stepped, and right-angled fracture angles show that depositional bone breakage took place (Lap 2020). This contrasts with the taphonomic faunal signals in the lower part of the BOS layer (Bos Three). It is thus very likely that there was an occupational hiatus after the formation of the BOS soils contributed to these taphonomic signals. Secondary carbonate precipitation, including speleothem formation, occurred during the occupational hiatus, after the formation of the BOS layers, and this was associated with increased amounts of dripwater that also led to loosening the base of the stalactite that fell into the deposits. Butzer (1982: 37) commented that there was “active stalagmite accumulation, leading to cementation” and local calcrete “lenticles” in layer 17, the equivalent of BOS. He observed evidence for the abundance of water during the formation of this layer and suggested that this indicates a substantially wetter climate during this period (Butzer, 1982: 39). An analysis of ostracods in the sediment indicated freshwater to slightly saline conditions (Faul, 2021).

Layer SBLs consists of very dark silty sand with patches of clay comprising part of the matrix. In contrast to SMONE and BOS, this layer contains intact combustion features with ash

layers preserved. SBLS is currently under excavation, but the shellfish reported on here is from around 5 cm thickness of deposit in square C1. This layer is attributed to another member that will be further discussed in the future.

3.4 Shellfish analysis

The methods employed to analyze the shellfish from these layers are discussed in detail by Brenner et al. (2022). The shellfish data reported complement those by Brenner et al. (2022), but this sample is slightly larger. Although the BOS layers have been discussed separately by Brenner et al. (2022), they are combined in this study. The layers were initially separated to interrogate site formation processes. However, as the deposit volume in BOS One and BOS Two is low, faunal exploitation patterns are best discussed for all the layers combined. Incidentals (non-food species) are not included in the taxonomic discussion here. The minimum number of individuals (MNI) and the weight values were calculated, and the maximum diameter of *Turbo sarmaticus* (alikeukel) opercula was measured using a digital caliper. Most of the shells were highly fragmented and decomposed, and there were no complete specimens of limpets and brown mussels available to measure. *Patella* sp. include fragments of limpets such as *Scutellastra longicosta*, *Scutellastra argenvillei*, and *Cymbula oculus*, which could not confidently individually be identified to species level because of their fragmentary state.

4 Results

4.1 Micromorphology and microanalysis

The 11 samples described in this study provide a range of shell middens (or middens containing shell) and shell-rich layers of various cultural contexts and from different areas of the main site. Some observations of the site-scale formation processes help contextualize the samples. Six of the blocks were collected from the Witness Baulk area of Cave 1, which is located well inside the chamber where the deposits are protected from open-air processes such as rainfall, overland flow, and winnowing by the wind. This area is, however, impacted by aeolian deposition and internal cave processes such as roof collapse events, dripping water, speleothem formation, and localized ponding. Whether this area could have been impacted by seawater inundation during storm surges is unknown, but this process has been proposed by Butzer (1982). Three of the blocks were collected from the area where the cliff-face overhang that forms Cave 1A meets the dripline of Cave 1. In this area, the deposits are also protected from rainfall. One block was collected from Cave 1A. Deposits in this area are somewhat protected from rainfall, depending on the wind direction. However, they are exposed

to overland flow, colluvial processes, and deposition of biogenic wastes by birds of prey that roost along the cliff face. Finally, two blocks were collected from the interior of Cave 2, which was protected from rainfall but was differentially impacted by diagenesis and either the formation of speleothems or dissolution of carbonates as a result of dripwater of variable acidity entering the cave's eastern and western sides. The diagenesis in Cave 2 has been previously described by Deacon and Geleijnse (1988) and Feathers (2002), and its impacts on the preservation of shell are described in this study at the microscale.

4.1.1 Cave 1 Witness Baulk: MSA I and MSA II/ Mossel Bay lower

The four blocks from the MSA I deposits of Cave 1 Witness Baulk (LBS member) contain abundant shell fragments visible in the thin section, particularly in the lowest two blocks. During sampling, the shells were exceptionally fragile and soft and could be easily cut through with a knife. The shells are roughly horizontally oriented and distributed in discrete layers interbedded with layers of charred material overlain by wood ashes, layers of mixed debris that include fragments of bone, and thin lenses of sand. Many of the shells are fragmented in place (Figures 4A,B) with a displacement of originally curved portions onto a roughly horizontal plane, an indicator that significant compression has occurred. Observations of the shell fragments at high magnification revealed that many are internally porous due to decalcification (Figures 4C,D). In some cases, porosity is greater in the fibrous layer relative to the nacreous layer, whereas the opposite is true in others. When present in association with ashes and charred plant material, the shells are darker gray in color under PPL, and some exhibit delamination or exfoliation planes (Figure 5). Other shells in ash layers are visibly recrystallized. μ FTIR analyses reported previously by Larbey et al. (2019) showed that one layer of shell fragments associated with a hearth in these samples was impacted by heating above 400°C, the temperature at which biogenic aragonite converts to calcite (Yosioka and Kitano, 1985). The observations of delamination and recrystallization show that heating may have also impacted the structural integrity of the shell.

Although some secondary minerals are present, these are limited to small hydroxyapatite ($\text{Ca}_{10}(\text{PO}_4)_6(\text{OH})_2$) nodules, thin phosphatic crusts, and zones of alteration of wood ashes. In places, ashes are replaced by hydroxyapatite in close proximity to shell fragments that are unaffected. Minor amounts of gypsum ($\text{CaSO}_4 \cdot 2\text{H}_2\text{O}$) are also present in the LBS deposits (Figures 4K,L), and there are a few examples of gypsum crystals formed within exfoliation planes in the shell. In addition, halite (NaCl) crystals form on the cut surfaces of the micromorphology blocks within weeks of slicing, which indicates that halite crystals are likely present in the samples. However, information about their spatial distribution has been lost due to dissolution during thin section production. The presence of gypsum and halite and the

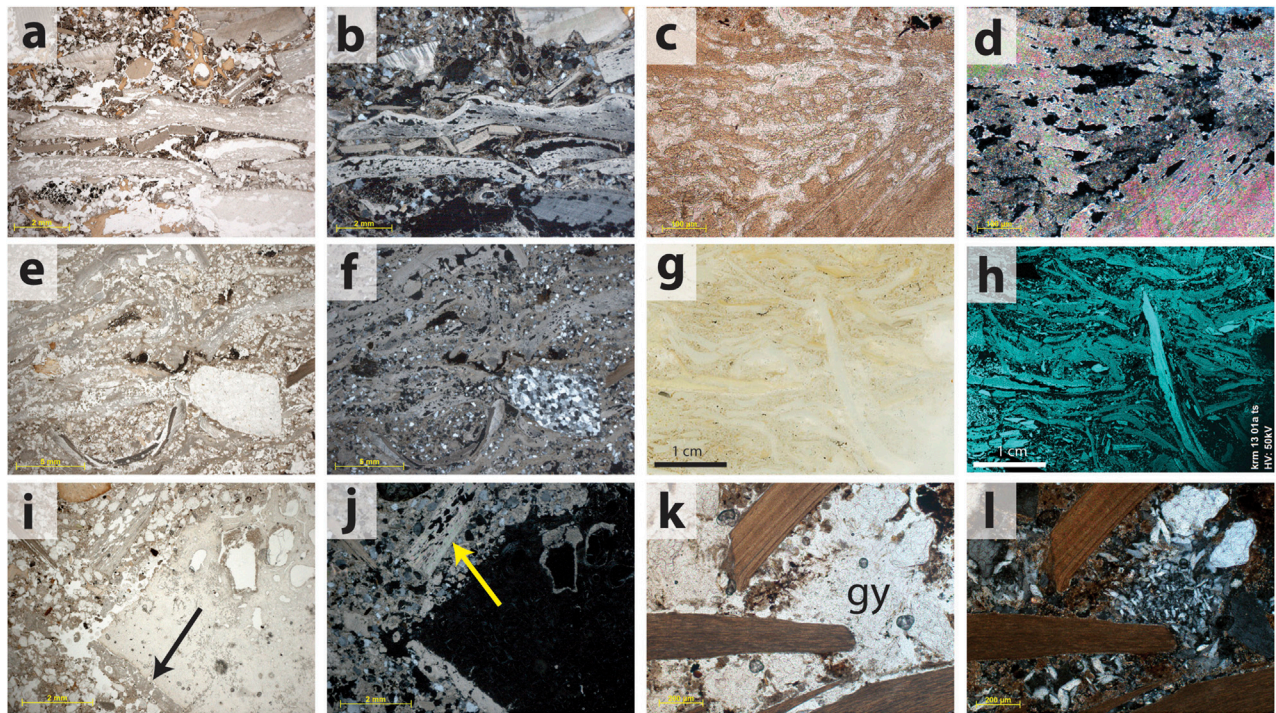


FIGURE 4

The dominant taphonomic processes impacting shell in the MSA deposits of Cave 1. **(A)** This sample from the Witness Baulk contains at least 8 discrete shells, illustrating a range of internal porosity due to decalcification, as well as fragmentation and deformation in place. PPL. **(B)** Same view as **(A)**, XPL. **(C)** High magnification detail of a shell composed of aragonite that has internal porosity due to decalcification. PPL. **(D)** Same view as **(C)** XPL. **(E)** Sample from the MSA I deposits located at the point of connection between Cave 1 and Cave 1a (KRM-13-01). Although difficult to see due to the calcareous matrix, over 50% of the image is composed of horizontally oriented shell. PPL. **(F)** Same view as **(E)**, XPL. **(G)** Incident light scan of a thin section from sample KRM-13-01. **(H)** An elemental distribution map of calcium produced from the same area as **(G)**. Here, the shells and their abundance are easier to see compared to the photomicrographs, and the shells composed of aragonite exhibit a lower Ca abundance relative to the shells composed of calcite. One particular shell composed of calcite is oriented vertically, and the shells composed of aragonite are deformed over its pointed edge. **(I)** A fragment of bone from sample KRM-13-02 exhibits a pendant of secondary calcite (arrow). PPL. **(J)** Same view as **(I)**, XPL. The arrow indicates a porous shell fragment. **(K)** Three relatively well-preserved shell fragments from the base of the Witness Baulk have a nodule of secondary gypsum (gy) in between them. PPL. **(L)** Same view as **(K)**, XPL.

association between gypsum and shell could indicate that secondary precipitation of gypsum and other soluble salts contributed to some of the fragmentation we see today.

At the top of the sequence, in the SASL sub-member, corresponding to the contact with the SBLS, soft-sediment deformation under conditions of high moisture, perhaps related to the stalactite that fell into the overlying deposits, has impacted the hearths and the layers containing shell. Ash layers at the contact with the SBLS show optical evidence of phosphatization with yellow color in PPL and isotropic zones in XPL, with μ FTIR analysis showing a more extensive presence of the mineral hydroxyapatite. The layers were deformed after phosphatization, suggesting a period of weathering, exposure to phosphatic materials such as guano under conditions of high moisture, and then deformation related to rockfall coincident with the SBLS. Phosphatization rims are observed on speleothem fragments, and some bones are internally recrystallized to an unknown mineral. One fragment of the operculum is observed to

also have phosphatized edges, whereas the remainder of the shells in this portion of the sequence have a stronger brown color in PPL and exhibit less internal porosity compared to samples lower down. The shell fragments in this sample comprise less than 50% of the area and are therefore not abundant enough to qualify this portion of the deposit as a midden.

4.1.2 Cave 1/1A interface: MSA I and MSA II/ Mossel Bay lower

Of the three blocks at the interface between Cave 1 and Cave 1A, the lowest, which is associated with MSA I cultural materials from the LBS member, contains shells that are fragile and soft. The upper two blocks contain much larger shells that are well-preserved and can only be cut through with the help of a hammer and chisel. These two blocks are from the same member and are the approximate lateral equivalent to the shell midden layers analyzed and dated in this study. However, due to the removal of sediment during previous excavations, there are issues with

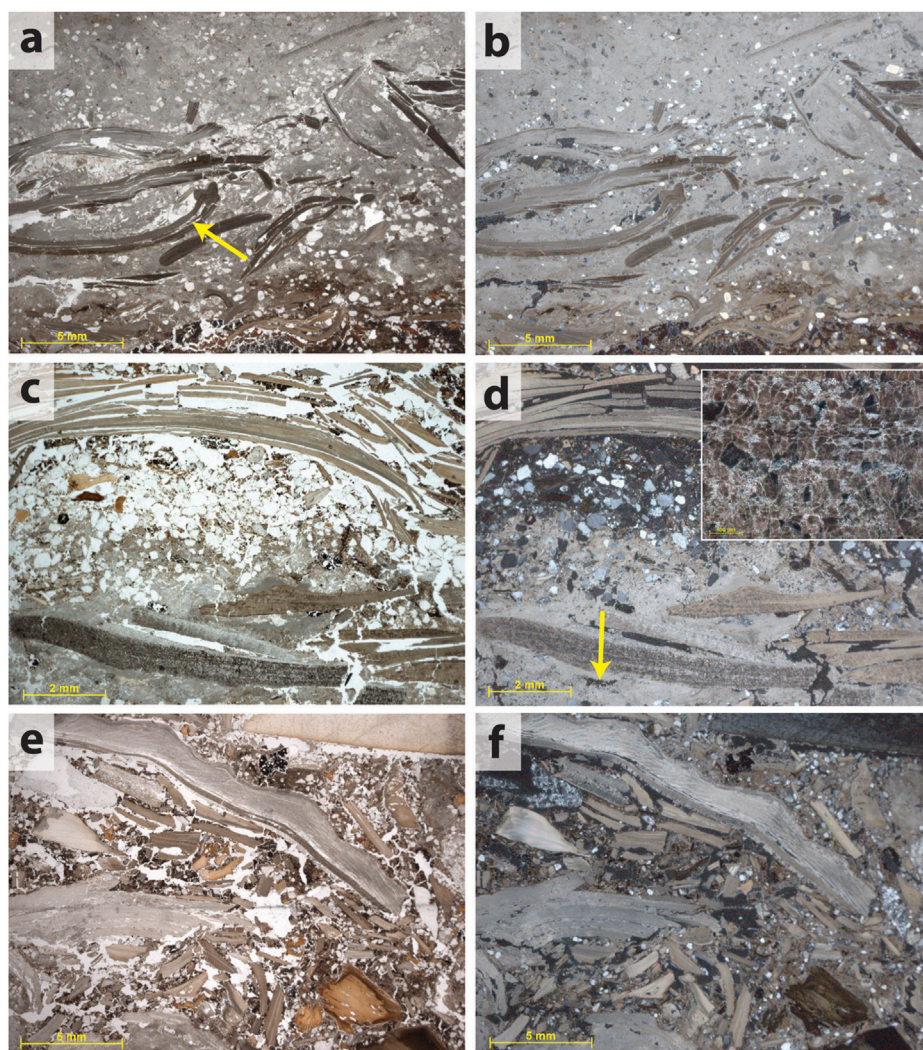


FIGURE 5

Impacts of human activities on the preservation of shell. **(A)** Burned shells in a hearth, sample KRM-13-07 from the LBS of Cave 1. According to the results of the μ FTIR analyses, all of the shells in this hearth are now composed of calcite due to heating [see also Larbey et al. (2019)]. Burned shells are also darker in PPL, ranging from medium to dark grey in color. Here, some shells exhibit delamination. The arrow indicates a fissure void formed within a bivalve shell from delamination between the inner nacreous and outer prismatic layers that extends to the hinge plate. PPL. **(B)** Same view as **(A)**, XPL. The fine matrix surrounding the shells is ash, while a small portion of the basal charred layer of the hearth is visible in the lower left corner. **(C)** The lower part of the image shows shells embedded in the ash layer of a hearth located several cm below the previous images. The shells are both heated and recrystallized. A similar change in orientation of calcite crystals has been reported in heated shell by Villagran et al. (2011b). The upper part of the image shows shells that are fragmented in place due to compression, possibly related to trampling (c.f. Villagran et al., 2011a). μ FTIR analyses indicate that all of the recrystallized shells within the hearth are composed of calcite, while the upper fragmented shell is composed of aragonite. PPL. **(D)** Same view as **(C)**, XPL. Arrow indicates a small zone of phosphatized ashes, confirmed as hydroxyapatite with μ FTIR. The inset image shows the recrystallization of one of the shell fragments at high magnification, also XPL. **(E)** This image from KRM-13-06a (also in the LBS) shows the impact of fragmentation due to trampling followed by local reworking of shell with other wastes, including fragments of bone, ash and charcoal. μ FTIR analyses indicate that the bone fragments visible in this image were burned at a range of intensities. PPL. **(F)** Same view as **(E)**, XPL.

correlating the layers directly. Sedimentary differences possibly reflect lateral facies changes or variations in nature and the degree of post-depositional color change.

Unlike the nearby deposits in the corresponding area of the Witness Baulk, the deposits in the lowest block are clast-

supported by shell fragments (Figures 4E–H) with a fine matrix composed of wood ashes and sand cemented in place by secondary carbonate. *In situ* layers of charred plant material and ashes are not present. Nevertheless, charcoal and partially recrystallized ashes are present in the

poorly sorted sedimentary matrix, suggesting that these materials were redeposited from a location where both shells and hearths were present. Large fragments of lithic debitage are also present. The sampled midden deposit can be divided into two main shell-rich units with geogenic sediment in between. In addition, thin lenses of geogenic and biogenic material, including sand-sized hydroxyapatite nodules that are typical of bird guano, are present within the two main units, suggesting that the thicker shell-supported units accumulated intermittently with pulses of non-anthropogenic sediment. Many of the shells appear deformed, and many have internal porosity. μ FTIR analyses indicate that these shells are composed of aragonite.

The two blocks laterally equivalent to the SASL contain much larger shells mixed with coarse fragments of other materials, including charcoal, bones, tufa, and quartzite clasts. The coarse nature of these units is consistent with the SASL layers in the Witness Baulk. Like the lower sample from the same area, the deposits are variably cemented with secondary calcite, which forms pendants on some bone fragments (Figures 4I,J) and infills bone pores. Shell fragments in these samples are generally well-preserved, but some show increased internal porosity suggestive of decalcification.

4.1.3 Cave 1 Witness Baulk: LSA

One block from the LSA shell midden from the Witness Baulk in Cave 1 provides a contrast to the MSA I and earliest MSA II deposits. This sample contained so many large shells that it was carved with a hammer and chisel. Like the earlier deposits, this midden contains layers of shell, as well as other layers containing mixed debris such as bone fragments (consistent in appearance with fish, see Villagran et al., 2017) and lenses of sand. Relative to the MSA I deposits, the intact shell layers have large amounts of void space, with much of the original morphology and curvature of the shell fragments preserved. This sample, with its large voids, exemplifies the compression and volume loss that must be accounted for in the earlier MSA deposits, which have the effect of making those middens thinner in appearance.

4.1.4 Caves 1A and 2: Howiesons Poort

The one sample from Cave 1A comes from the base of the Upper Member with Howiesons Poort artifacts in a midden context where shells are present but do not form the dominant component of the midden. In the field, the feature is dark gray. In the thin section, the feature contains four discrete microstratigraphic units that contain different proportions of materials, including fragments of shell, bone, burned bone, fat-derived char, wood ash, charcoal, charred seeds, quartzite clasts, fragments of tufa, and sand. The units also vary in

porosity. The uppermost unit is composed of abundant wood ashes, which are locally recrystallized and cemented by secondary carbonate. The other unit boundaries show no evidence of decalcification or lenses of geogenic sediments that would suggest periods of stasis between depositional events.

The interpretation of this sequence is that of a midden that contained dumped materials from primary features, such as hearths, mixed with other types of food-related debris. Although shell fragments are present, this feature is not considered to be a shell midden. Decalcification is present only at the very top of the feature, and, in general, this midden is well-preserved.

In Cave 2, at a slightly higher stratigraphic position compared to the sample from the Upper Member in Cave 1A, the sample from the western side contained large visible shells in the field, which required a hammer and chisel to cut into for block removal. Visible flowstones were also present nearby. The sample from the eastern side of the chamber contained no visible shell, and the deposits were dark brown, greasy, soft, and easy to cut, with visible bands of sediment grading laterally from white to yellow, including what appeared in the field to be a phosphatic mineral crust or phosphatized flowstone.

The sample from the western side of the cave is illustrated in Figures 6A–F and contains two thick (~2–3 cm) packages of sediment that are composed almost entirely of shell fragments (>50%), as well as one thinner layer that contains large fragments of shell mixed with other sediments. The lowest package of the shell is capped by a thin layer of secondary phosphate that, in places, is pseudomorphic after plant ashes. A thin layer of charcoal beneath suggests that the shell deposit was originally capped by an *in situ* hearth that subsequently became phosphatized. μ FTIR analyses indicate that the mineral replacing the original wood ashes is hydroxyapatite. The middle layer of the shell also contains evidence of secondary phosphatization, this time with direct replacement of the aragonite of the shell by hydroxyapatite. The very top of the sample is ashy sediment cemented by micrite, which is capped by a thin concentration of shell fragments that are embedded in the carbonate and exhibit thin calcite spar pendants. Overall, this sequence represents at least three main phases of shell deposition punctuated by the use of the same area for the construction of hearths and stasis during which weathering occurred. Despite being located in a zone of shell and bone preservation, the micromorphological analyses indicate that some degree of post-depositional diagenesis occurred here.

In contrast, the sample from the eastern side of the Cave 2 chamber contains no shell (with one exception illustrated in Figures 6H–J) or bone fragments, and the sand component is non-calcareous. Instead, the light-colored bands visible in the field contain the mineral leucophosphite ($\text{KFe}_2(\text{PO}_4)_2(\text{OH}) \cdot$

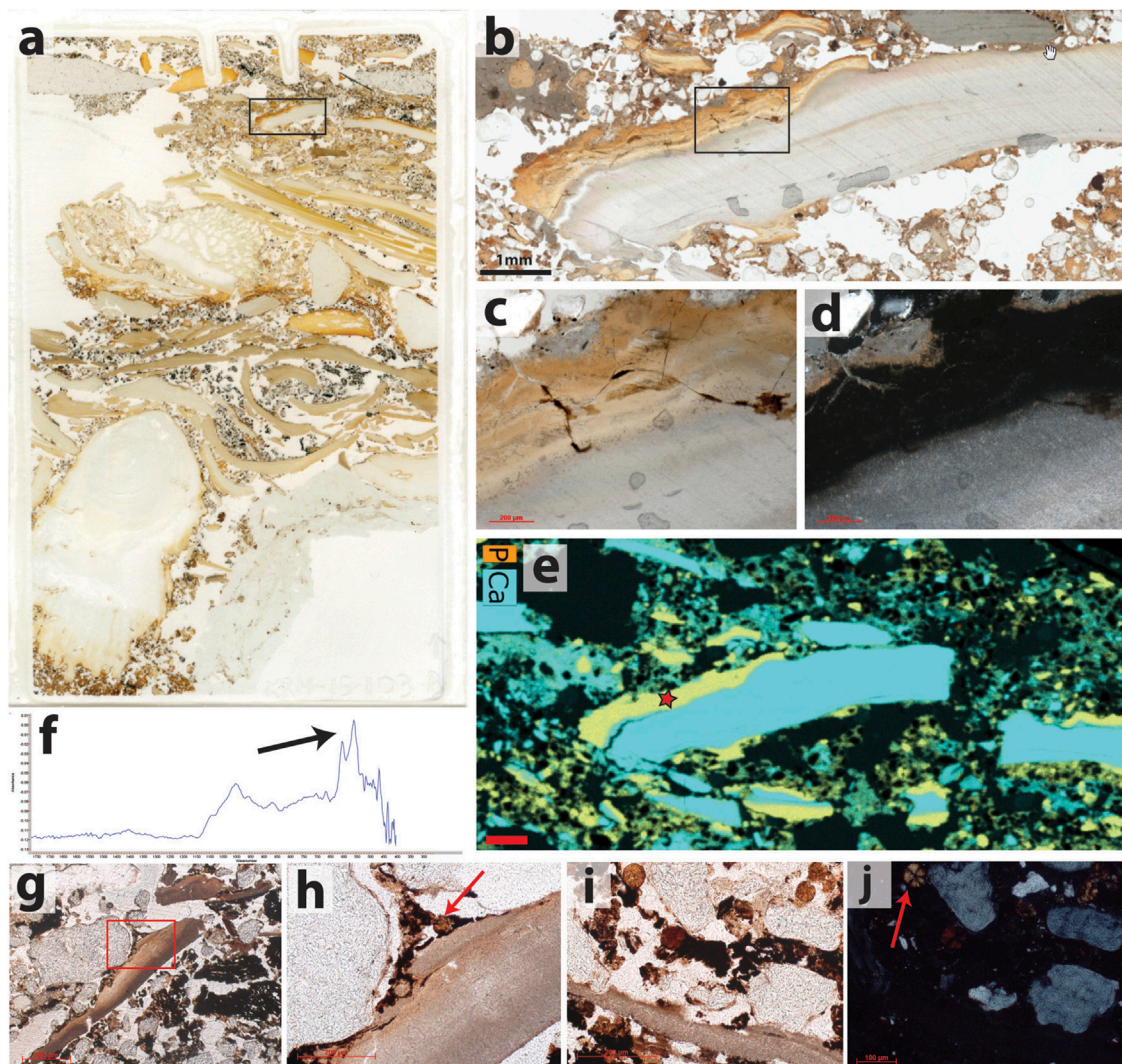
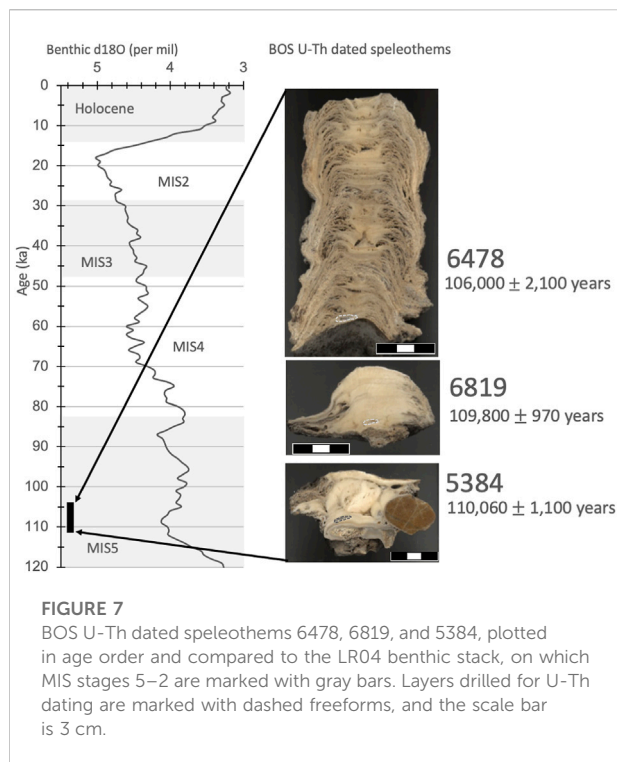


FIGURE 6

Phosphate-induced diagenesis of shell in Cave 2. **(A)** Flatbed incident light scan of a thin section from the preserved HP shell midden in Cave 2. Two distinct layers of shell are visible here, approximately 2 cm in thickness each. The lower shell layer is well-preserved and is composed of > 50% shell. The upper shell layer is more compressed, and has been impacted by post-depositional phosphatization. The box indicates the location of the photograph in **(B)**. **(B)** Detail of an altered shell fragment. PPL. The box indicates the location of the photographs in **(C,D)**. **(C)** Under PPL, the alteration zone is yellow. **(D)** Under XPL, the alteration zone is isotropic. **(E)** Distribution map of the elements Ca and P. The alteration zone contains both elements. The location of the μ FTIR measurement in **(F)** is indicated by the star. The scale bar is 1 mm. **(F)** μ FTIR spectrum collected directly off the thin section using a germanium ATR objective. The arrow indicates the position of the doublet at 605 and 565 cm^{-1} that is characteristic of hydroxyapatite. **(G)** The only shell present in the sample from the eastern side of the chamber is broken into multiple fragments, but retains its color in PPL. The matrix is rich in micro-charcoal. **(H)** Detail of the area indicated by the red box in **(G)**. The original fabric of the shell is preserved. The red arrow indicates a leucophosphite crystal aggregate. PPL. **(I)** One of the shell fragments located just to the right of the image in **(G)**, with five leucophosphite crystal aggregates above it. PPL. **(J)** Same view as **(I)**, XPL. The shell fragment is completely isotropic, but due to the presence of silica rather than hydroxyapatite. The radial crystal habit of the leucophosphite is visible here, with the well-developed extinction cross in one aggregate indicated with the arrow.

$2\text{H}_2\text{O}$) in a matrix of amorphous silica. The leucophosphite has a radial crystal habit (Figure 6J), and pseudomorphs of original calcareous materials, such as ashes or shells, are not present; however, the dark matrix is rich in finely comminuted charcoal, which suggests that hearths may

have been present. According to Karkanas et al. (2000), the combination of leucophosphite and amorphous silica is one possible diagenetic outcome of the exposure of wood ashes to phosphatic solutions, such as those derived from weathered bat or bird guano. The observations support the previous interpretations



of extreme post-depositional diagenesis and carbonate dissolution in this cave area. The diagenesis is so advanced that it is impossible to determine whether shell middens were located here. Relative to the sample from the western side of Cave 2, the sample from the eastern side has significantly lower porosity, which is one aspect of the deposits that Feathers (2002) considered when assessing the potential impacts of diagenesis on the OSL dating.

One possible microscopic shell was observed in the sample from the western portion of Cave 2. The shell, which had an original length of a maximum of 5 mm, is fragmented in place into more than ten individual pieces. It retains its typical gray color in PPL, but under XPL, it is isotropic. Elemental mapping reveals a depletion in Ca and an enrichment in Si, which suggests that this shell may be partially replaced by secondary silica. The μ FTIR spectrum is also consistent with the presence of opal. The shell is located in a layer of charred plant material directly beneath a concentration of leucophosphite. Although suggestive of another diagenetic process that impacted the heated shell at the site, this single observation would suggest that it is not a widespread phenomenon. Overall, the micromorphological analyses show a wide range of taphonomic processes that impacted the preservation of the middens.

4.2 Dating

The results of the U-Th dating, including all the isotopic concentrations and ratios, are presented in Table 2. U

concentrations for all three dated speleothem samples are 655–440 ppb (ng/g), which is not untypical for carbonates in archaeological settings (Hellstrom and Pickering, 2015). The similarity in U concentration hints at the same source of U for all three samples, as do the similar $^{234}\text{U}/^{238}\text{U}$ activity ratios. The $^{230}\text{Th}/^{232}\text{Th}$ ratios are all well below 30, but a detrital thorium correction was still applied, and the corrected ages are reported in this study. Sample 5384 is the oldest, with an age of $110,060 \pm 1,100$ years, which is within the error of sample 6478, dating to $109,800 \pm 970$ years. This is unsurprising as these two carbonate pieces are from the same archaeological horizon, BOS Three. Sample 6478 is the youngest, with an age of $106,000 \pm 2,100$ years, and is at least 2,000 years younger than the other two carbonates (Table 2).

All three speleothems consist of layers of dense white calcite with clear breaks, marked by very thin (under 1 mm) dark brown to gray layers (Figure 7). The dated layers in all three cases are from the base of the speleothem and therefore date as close to the onset of speleothem formation as possible. This means there was a time conducive to speleothem formation at KRM starting at $110,060 \pm 1,100$ years, lasting for around 4,000 years until $106,000 \pm 2,100$ years ago. The oldest sample, 5384, is best described as a carbonated mass and marks the beginning of an increase in dripwater to this part of the cave, which points to a shift to wetter external conditions. Within a thousand years, the increase in dripwater was sufficient to sustain the growth of a small stalagmite, sample 6819. By $106,000 \pm 2,100$ years, drip rates are fast enough to produce sample 6478, which, given its open textures, appears to have grown fast. There are several areas along the central growth axis of 6478 where some dissolution of the previous layer is evident, suggesting a very fast drip rate. Further dating is needed to constrain the length of time represented by 6478. However, taken together, these U-Th ages provide a maximum age for the hiatus after the formation of the BOS layer at around 106 ka and a minimum age of around 110 ka for Layer SBLS and the underlying layers.

4.3 Shellfish density and taxonomy in the Witness Bulk layers SMONE-BOS

The shellfish density in SMONE is the highest, at 90.3 kg/m^3 , followed by SBLS at 43.3 kg/m^3 , with BOS at a little lower density of 37 kg/m^3 (Table 3). The shellfish exploitation from SMONE is characterized by mainly two species in terms of MNI: alikreukel (47.5%) and brown mussel (41.4%). When the weight of marine shellfish is considered in SMONE, alikreukel still dominates, but abalone (*Haliotis midae*) is almost as numerous as the brown mussel. In BOS, brown mussel becomes the best-represented taxon in MNI (34.1%) and weight (23%). Alikreukel is still well represented in MNI (23.1%) and weight (32.8%), but whelks contribute almost as much in MNI (19.2%). Limpets (*C. oculus*)

TABLE 3 Shellfish MNI and weight; shellfish density and opercula size (median); and layers SMONE, BOS, and SBLS. The ecoprofile for the top > 85% taxa is indicated through light gray shading (sheltered conditions) and dark gray shading (exposed wave interaction conditions). The taxa are ordered according to rank in terms of handling costs (Langejans et al. 2012).

Layer Shellfish density Opercula size median	SMONE 90.3 kg/m ³ 35.7 mm (n = 47)				BOS 37 kg/m ³ 38 mm (n = 31)				SBLS 43.3 kg/m ³ 29.3 mm (n = 3)				Total			
	MNI	% MNI	g	%g	MNI	% MNI	g	%g	MNI	% MNI	g	%g	MNI	% MNI	g	%g
<i>Dinoplax gigas</i> (giant chiton)	0	0	0	0	4	1.7	11.4	0.8	2	4	12.7	3.5	6	1.3	24.1	0.6
<i>Turbo sarmaticus</i> (alikleukel, Cape turban)	94	47.5	1,036	52.1	53	23.1	447.4	32.8	6	12	48.5	13.3	153	32.1	1,531.9	41.2
<i>Cymbula oculus</i> (limpet)	1	0.5	11.8	0.6	4	1.7	110.1	8.1	3	6	19.7	5.4	8	1.7	141.6	3.8
<i>Diloma sinensis</i> (top shell)	1	0.5	9.3	0.5	44	19.2	142.1	10.4	3	6	33.7	9.2	48	10.1	185.1	5.0
<i>Donax serra</i> (white mussel)	1	0.5	5.6	0.3	2	0.9	3.7	0.3	1	2	11.1	3.0	4	0.8	20.4	0.5
<i>Perna</i> (brown mussel)	82	41.4	453.8	22.8	78	34.1	475.1	34.9	18	36	115.4	31.6	178	37.3	1,044.3	28.1
<i>Haliotis midae</i> (abalone)	4	2.0	369.2	18.6	2	0.9	11.6	0.9	0	0	0	0	6	1.3	380.8	10.3
<i>Scutellastra argenvillei</i> (limpet)	2	1.0	39.3	2.0	2	0.9	23.3	1.7	0	0	0	0	4	0.8	62.6	1.7
<i>Burnupena limbosa</i> (whelk)	10	5.1	11.1	0.6	29	12.7	77.1	5.7	11	22	34	9.3	50	10.5	122.2	3.3
<i>Scutellastra longicosta</i> (limpet)	1	0.5	0.3	0.0	2	0.9	8.2	0.6	1	2	1.2	0.3	4	0.8	9.7	0.3
<i>Patella</i> sp.	1	0.5	49.8	2.5	4	1.7	47.3	3.5	4	8	88.7	24.3	9	1.9	185.8	5
Other*	1	0.5	1.1	0.1	5	2.2	4.9	0.4	1	2	0.6	0.2	7	1.5	6.6	0.2
Total	198	100	1987.3	100	229	100	1,362.2	100	50	100	365.6	100	477	100	3,715.1	100

*"Other" comprises *Turritella carinifera*, *Aulacomya atra*, *S. barbara*, and *bulli* sp.

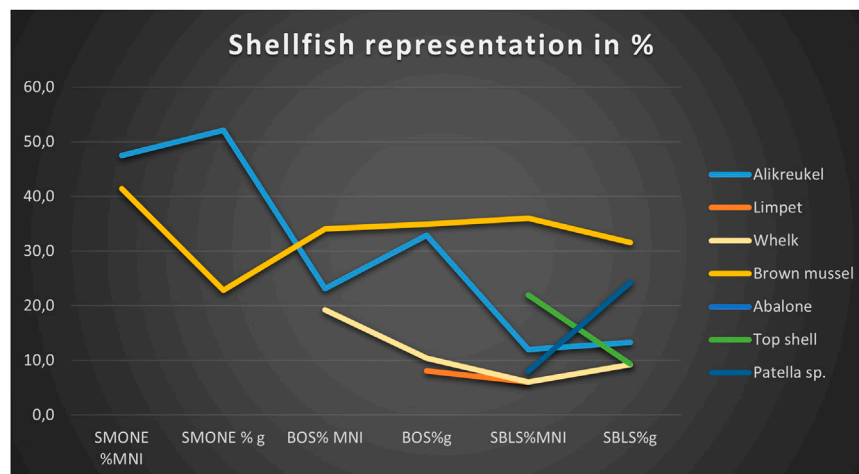


FIGURE 8 Shellfish representation SMONE-SBLS (top 85%–91%) (see Table 3 for percentages).

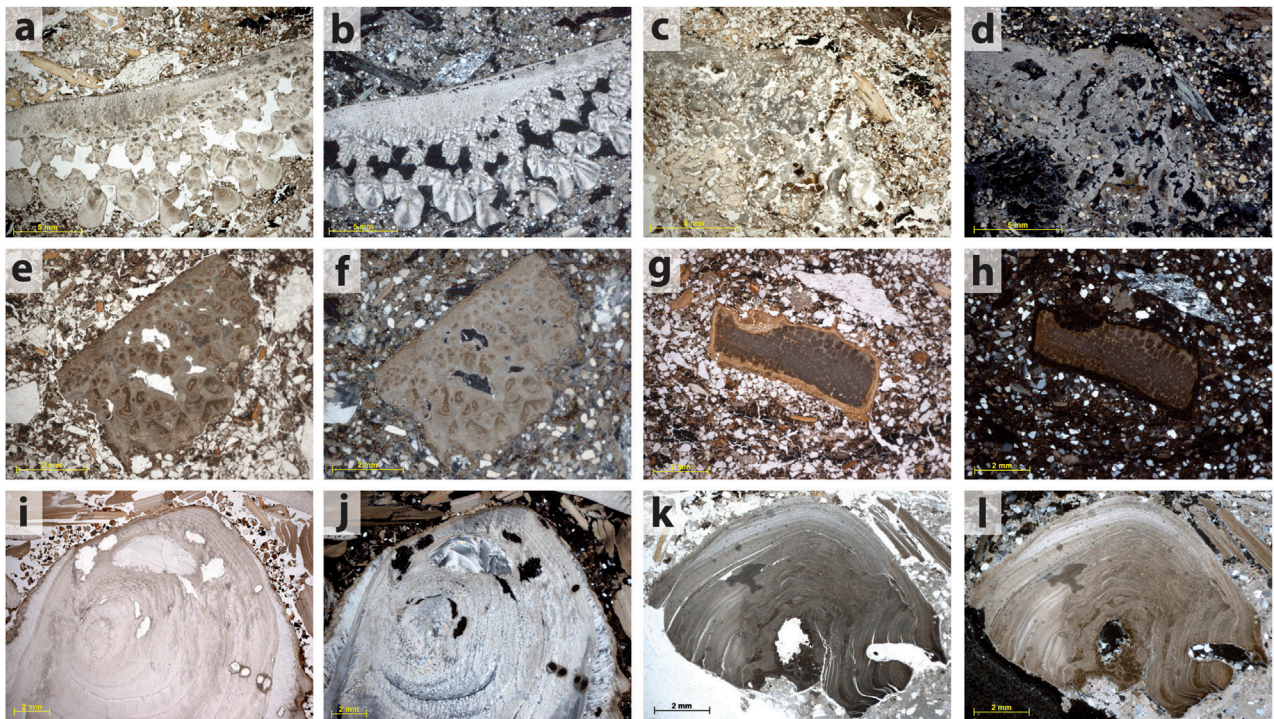


FIGURE 9

Differential preservation of opercula. **(A)** A well-preserved operculum from sample KRM-15-112, collected from the lateral equivalent of the SBLS. The inner part is oriented downwards. Porosity here is original. PPL. **(B)** Same view as **(A)**, XPL. The birefringence of the carbonate, and original crystallite orientation fabric indicates that the shell has not been chemically altered. μ FTIR analyses indicate that all parts are composed of aragonite. Inner part oriented downwards. **(C)** A partially dissolved, recrystallized and compressed operculum from sample KRM-13-08, collected within the LBS. PPL. **(D)** Same view as **(C)**, XPL. The porosity here is secondary, and nearly all of the original crystallite orientation fabric is lost, but the composition is aragonite. **(E)** An altered operculum from sample KRM-13-05, collected from the contact between the SBLS and the LBS. The color in PPL indicates possible heating, and the composition is calcite. Inner part oriented downwards. PPL. **(F)** Same view as **(E)**, XPL. The matrix contains quartz and carbonate sand, as well as ashes. **(G)** A different altered operculum, also from sample KRM-13-05, just below the contact between the SBLS and the LBS. The outer edge of the fragment has been replaced by secondary hydroxyapatite, confirmed with μ FTIR. PPL. **(H)** Same view as **(G)**, XPL. The matrix contains little carbonate and is enriched in microcharcoal and organic material. **(I)** A well-preserved operculum from sample KRM-15-103. This operculum—located in the eastern side of Cave 2—is composed of aragonite. The orientation of the cut is perpendicular to that of the previous images. PPL. **(J)** Same view as **(I)**, XPL. **(K)** A burnt operculum from sample KRM-13-07. The orientation of the cut is similar to that of **(I)** and **(J)**. PPL. **(L)** Same view as **(K)**, XPL. The matrix is ash.

and top shells (*B. limbosa*) also occur in relatively high percentages, contributing to the top 85% of species in this layer (Figure 8).

In SBLS, the brown mussel remains the best-represented species and occurs in similar proportions to those of BOS (36% MNI, 31.6% in weight). However, this layer stands out in the higher diversity of shellfish that make up the top 85% in this layer (Table 3; Figure 8). In terms of MNI, top shells almost comprise a quarter of the composition, with alikreukel, limpets, whelks, and *Patella* sp. occurring in similar proportions. The weight representation better indicates that *Patella* species have been an important part of the diet, representing 24.3% of the total weight. Figure 8 shows the increased importance of alikreukel over brown mussels in the youngest layer, SMONE, the switch to brown mussels as the most represented species in BOS and SBLS, and the increasing diversity of shellfish representation in the older layer, SBLS.

5 Discussion

5.1 Taphonomy of shell middens at KRM

The presence and positioning of shell middens in caves and rock-shelters can expose the archaeological materials to negative taphonomic processes, such as secondary phosphatization and complete dissolution. However, they can provide contexts favorable to rapid burial and protection of archaeological materials, and depending on the sedimentation rate, either cemented deposits or speleothems for dating.

At KRM, various taphonomic processes were observed impacting the shells and shell middens. Some of the processes documented here at the microscale and, to a lesser extent, during excavation include the syndepositional effects of anthropogenic activities. Micromorphological analyses of the LBS middens in

the Witness Baulk and nearby profiles revealed a range of anthropogenic activities. Construction of hearths on top of shell layers and possible discard of shell directly into the fires resulted in burning, which caused a color change, thermal fracture, change in mineral composition, and recrystallization. In addition, some *in situ* fragmentation and compression of the shell may be attributed to trampling. Finally, the thicker, poorly sorted, clast-supported deposit at the intersection between Cave 1 and Cave 1A shows that the shell and other materials were removed from their original place of processing and redeposited by humans.

Other taphonomic processes resulted in shell dissolution and degradation. In many samples from Cave 1, partial dissolution caused an increase in internal porosity visible only at the microscale. Dissolution is a common process in shell middens worldwide (Aldeias and Bicho, 2016; Duarte et al., 2019). In open-air sites, dissolution can be initiated by localized acidic conditions within the mounds that result from the decomposition of organic material coupled with a terrestrial moisture source (Stein 2008). This mode of dissolution may have impacted the upper surface of the LBS deposits, as well as the SMONE, BOS, and SLBS layers studied here. At greater depth, dissolution also occurred within alkaline sediments rich in ash, which suggests that the process at KRM might be more complicated than in open-air sites.

Dissolution may have preferentially impacted shells composed of aragonite, particularly the thinner shells of the brown mussel (Deacon 1995). However, Figure 9 illustrates differences in the preservation of opercula (an anatomical portion that is absent in brown mussels) in all of the different areas of the site, with one operculum from the LBS exhibiting a similar degree of decalcification as the brown mussel shells (Figures 9C,D). The partially dissolved shells were then more susceptible to compression and soft sediment deformation. These effects lead to a transformation from a highly porous clast-supported shell deposit to a “dominant interconnected shell” deposit (Aldeias and Bicho, 2016), wherein shells are fragmented in place, with loss of the original void space resulting from the internal chambers and concavity of the shells. Partial shell dissolution is a process that can be observed in hand samples and during excavation.

In Caves 1 and 2, phosphatization impacted calcareous materials, including shells. This process occurred at the top of the LBS deposits in the center of Cave 1. In Cave 2, lateral variation in dripwater composition resulted in one area where shells are relatively well-preserved but locally phosphatized with the replacement of the original aragonite by hydroxyapatite. However, in the other areas, shells have been completely dissolved, yielding a decalcified deposit containing the secondary mineral leucophosphate.

Finally, the precipitation of additional secondary minerals may have contributed to the fragmentation of the already fragile shell. Delamination, or fracture along the growth

layers, appears to be common in certain species and can be caused by heating (Villagran et al., 2011a) and precipitation of secondary salts, a process that impacts the lowest deposits of the Witness Baulk. Other secondary precipitates include secondary carbonate, which forms pendants and encrustations on the shell and bone at the connection point between Cave 1 and Cave 1A, as well as in the eastern area of Cave 2. In the Witness Baulk, a hiatus in sedimentation, coupled with precipitation of secondary carbonate from dripping water, resulted in the formation of crusts and stalagmites, which were directly dated here.

Overall, the shell analyses presented here from the SASL and underlying SBLS layer also show that despite some issues of preservation that have impacted both shells and other calcareous materials such as ashes, valuable information about fluctuations in species abundance can still be obtained when the deposits are excavated carefully. Nevertheless, the preservation issues have impacted the perception of the scale and, therefore, the potential for the interpretation of the action of shellfish collecting, consumption, and discard at the site. Marean (2014), for example, noted the poor visibility of deposits or layers that would technically qualify as shell-supported middens based on field observations of profiles. The taphonomic processes documented here help us to understand why shellfish remains are not necessarily obvious in profile and why the differential recovery has hindered the publication of high species counts, which, for example, are used to evaluate the lower intensity of MSA shellfish collection relative to the LSA (Will et al., 2019). Marean (2014) suggested different strategies for documenting shell density in different layers. In Figure 10, we use the micromorphology samples to illustrate the abundance of shell relative to other components in four middens from the site, three of which contain layers with greater than 50% abundance. One of the most striking differences is between the middens of the LBS (Figures 10B,C) and those of the Holocene (Figure 10A), wherein it is very clear that much volume has been lost in the LBS deposits due to the reduction of void space, compaction of the shell, fragmentation of the shell, and deformation coupled with decalcification. Other metrics for documenting density include counts and weights of shells, as well as piece plotting, which are addressed in the excavation data presented here and by Brenner et al. (2022).

5.2 Significance of middening and dumping

Deacon (1995: 126) noted that one of the most significant aspects of one of the MSA II shell middens in Cave 1A is that it is evidence for “patterned disposal of food refuse in localised heaps.” He emphasized this point as equally important as the systematic use of coastal resources. Middening, in the form of sweeping and dumping of hearths, is a well-established behavior

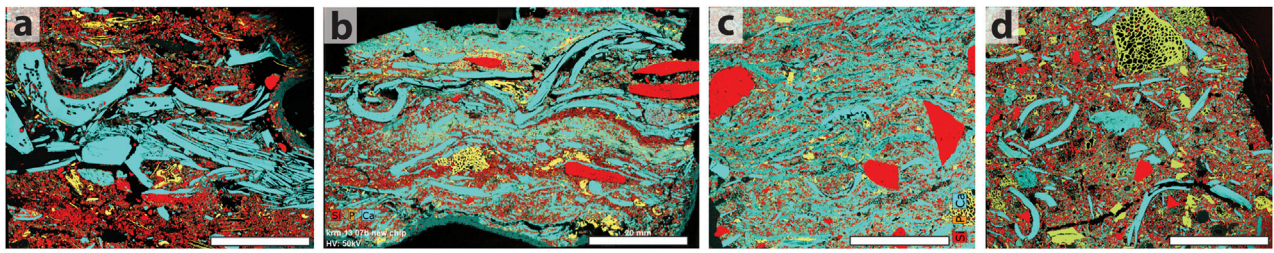


FIGURE 10

Fabric analysis of middens using compositional maps showing the distribution of the elements Ca, P and Si. In these images, shell, ash and secondary carbonate are blue; sand and quartzite are red, and bones are yellow. All images are the same scale; the scale bar is 2 mm. **(A)** LSA midden in Cave 1 (sample KRM-13-25) showing a discrete layer composed only of shell debris in between two layers rich in quartz sand with inclusions of bone. Several of the larger shells contain tubular pores that form as a result of invertebrate boring. Shell fragments are roughly horizontally aligned. **(B)** MSA I midden in the LBS deposits of Cave 1 (sample KRM-13-07) showing multiple discrete layers containing more than 50% shell interbedded with lenses of sand, mixed debris layers containing quartzite, shell, sand and bone, and layers of ash. Shell, quartzite and bone fragments are roughly horizontally aligned. Many of the shells are fragmented in place. **(C)** MSA I midden in the LBS deposits where the Cave 1 and Cave 1a deposits connect (sample KRM-13-01) showing no discrete layers. Shells are roughly horizontally aligned and embedded in secondary carbonate and ashes, yet still comprise greater than 50% of the deposit. In this sample, there are as many as eight shells per cm of thickness, which indicates significant post-depositional compression. Quartz sand is mixed throughout and the large fragments of quartzite debitage have random orientations. Under the microscope, fragments of charcoal and recrystallized ashes are also randomly mixed. This type of midden is interpreted as a reworked version of **(B)**. **(D)** HP midden in Cave 1a (sample KRM-13-13) that is rich in shell (<50%), but is not classified as a shell midden. Here all materials including the shell fragments have random orientations, suggesting that these materials were scooped up from their original place of deposition and dumped here.

in other MSA sites (Goldberg et al., 2009) that has been interpreted as evidence of intensification of site occupation, and in caves, the organization of activities within a more limited space. Herein, we see middening occurred in the same location as habitation, beginning in the MSA I and continuing through the HP (Figures 5, 6), evidenced by interbedded layers of discarded shell, *in situ* hearths, and locally reworked and trampled materials. Additionally, we see discrete areas used as dumps (Figures 4E–H and Figure 9D). Finally, the microstratigraphic observations and excavations reveal evidence for frequent hiatuses in anthropogenic sedimentation, which can be interpreted as periods of site abandonment that, in the case of the SASL layers discussed here, coincided with a phase of dripping that resulted in the formation of stalagmites observable in all the areas of Cave 1.

5.3 The paleoclimate and environment during MIS 5c-d

Altogether, the speleothem U-Th ages presented here provide a time window from $110,060 \pm 1,100$ to $106,000 \pm 2,100$ years ago, during which cave conditions were conducive to speleothem growth. Drip rates into the cave increased, and the influx of sediments into the cave decreased, as sedimentation and speleothem formation are mutually exclusive for the most part (Pickering et al., 2007). The oldest sample, 5384, is a carbonated mass, suggesting that, at $110,060 \pm 1,100$ years ago, we saw the onset of increased dripwater flow, but this may not have been enough to sustain the growth of even small stalagmites. We only

saw these around 1,000 years later. This period of increased drip flow is then sustained for the next 4,000 years, as evidenced by the age of 6478 at $106,000 \pm 2,100$.

The conditions during speleothem formation at KRM between ca. 110 and 106 ka relate to a period when increased moisture was available. The Tswaing crater lake pollen record indicates a wet phase between 111 and 103 ka (Partridge et al., 1997; Kristen et al., 2007). The data from the marine mud core, CD154 10-06P, that track the Agulhas Current near-surface temperature and salinity (Simon et al., 2015, 2020; Cawthra et al., 2021) correspond closely to those from the Tswaing crater lake. An explanation for this wet phase, suggested by Simon et al. (2015), is the role of the 19-23 ka orbital precession cycle, driving stronger summer insolation and, in turn, increased precipitation over eastern South Africa. This may be supported by other evidence from the Vankersvelsvlei coastal wetland pollen record, which also suggests an increase in summer rain during this period and that this allowed the development of a more extensive forest in the area (Quick et al., 2016). Analyses of spores, pollen, and micro-charcoal from the IODP Site U1479 deep-sea sediments, which capture the regional signal for the southern and western Cape GCFR (Dupont et al., 2022), further support that the presence of Podocarpaceae (occurring in Knysna type forests) increases substantially after the Last Interglacial maximum at 125 ka. This collection of local and more distant records is consistent with the presence of the small stalagmites in BOS, which by their presence alone suggest an increase in local effective precipitation.

Serial $\delta^{18}\text{O}$ measurements of the alikreukel opercula from AA43 in Cave 1/1A show that sea surface temperatures were not

depressed during this period and that the mean temperature was 13.2°C (Loftus et al., 2019). Alikreukel were collected mainly in summer (Loftus et al., 2019). It remains to be explained why the average alikreukel opercula size is smaller in all of the MSA II layers than in the rest of the MSA as indicated in the Singer and Wymer sample (Steele and Klein, 2008; Klein and Bird, 2016), the Deacon sample (Thackeray, 1988), and the opercula from SMONE-SBLS. The smaller size may relate to lesser food availability in relatively warmer waters (Sealy and Galimberti, 2011; Langejans et al., 2017) or, as suggested for the Holocene, to increased human predation (Klein et al., 2004). An increased estuarine component in the environment, as reflected by the fish in the Mossel Bay lower, may also be one of the factors involved in the decreased opercula size (Langejans et al., 2017: 72). The relatively smaller size is not only related to alikreukel opercula, as a sample of white mussels from the earlier MSA II/Mossel Bay phase at KRM is also smaller than those from after 90 ka (Jerardino and Navarro 2021). This same trend has been observed at PP 13 B aggregate LRS and a contemporaneous assemblage from Herolds Bay Cave, but larger samples are necessary to fully test this.

The fauna from KRM indicates that more closed environments, in which trees and shrubs dominated, prevailed during the formation of the MSA II/Mossel Bay phase (SAS member) as a whole. Relatively more browsers and mixed feeders occur, and lower ungulate diversity values may indicate increased forest elements in the environment (Reynard and Wurz, 2020). For the MSA II lower specifically, small mammals (size 1) are the most prevalent large mammal fauna (LMF) and, with seals occurring second most frequently, demonstrate that the coast remained close to KRM during this phase.

5.4 Coastal exploitation prior to 100 ka on the South African coast

The most abundant species targeted in the MIS 5c-e layers at KRM, PP 13B, HDP 1, and YFT 1, such as mussels, alikreukel, and limpets, are highly ranked as they provide relatively high amounts of meat yield in relation to handling cost (Langejans et al., 2012). This focus on a relatively narrow range of species exploited by these populations is similar to that observed for modern coastal foragers from SA and Australia (Kyriacou et al., 2015).

For the deposits older than 100 ka from KRM discussed here, there are differences in the shellfish density, proportional changes in the shellfish taxonomy indicating changing coastal ecologies, and shifts in the lithic technology. SMONE has the highest shellfish density and is dominated by alikreukel, which with abalone, comprise 70% of the taxa. This points to the availability of rock pools with sandy substrates sheltered from wave action. This coastal ecology is similar to that of the Deacon sample for the MSA II/Mossel Bay lower from Cave 1A

(Langejans et al., 2017). The shell midden from SMONE is associated with lithics from all stages of the reduction system, and many tools have edge damage (Brenner et al., 2022). Layer SMONE reflects coastal foraging similar to the Blombos Cave M3 phase (ca 97–82 ka) and MIS 5c PP 13B (ca 91–101 ka) in terms of the narrow range of taxa exploited, mainly alikreukel at the former and white mussels, brown mussels, and alikreukel at the latter (Jerardino and Marean, 2010; Langejans et al., 2012; Brenner et al., 2022). Similar shellfish densities do not occur at all southern Cape sites during this period—the shellfish density in SMONE and BBC M3 is similar, but noticeably lower densities occur in PP 13B MIS 5c layers. Furthermore, BBC M3 and PP 13B MIS 5c assemblages have a much lower proportion of artifacts per liter of sediment than SMONE, but the assemblage composition and technology are broadly comparable. The lithic density and characteristics coupled to the shellfish density suggest that KRM was used as a residential site during the formation of SMONE (Brenner et al., 2022) and that perhaps BBC and PP were less frequently visited during this period.

For the older than 110 ka BOS layer, the shellfish density is less than half that of SMONE, and a change in the coastal ecology toward more rocky exposed conditions is indicated by an increase in brown mussels, a concomitant decrease in alikreukel, and a greater variety of taxa (Figure 8). The higher artifact density in this layer and fewer edge-damaged pieces relative to SMONE may show that residential occupation may have been less intensive during this phase. In the pre-110 ka SBLS layer, similar shellfish densities occur as in BOS, but the diversity of taxa is higher. As in BOS, a rocky exposed coast is reflected, but to a larger extent. The shellfish density in BOS and SBLS needs to be interpreted against the significant taphonomic impact of dripwater and calcification, leading to the alteration and dissolution of the shellfish. The artifact density is much higher in SBLS than in SMONE and BOS, and miniaturization of the lithics occurs. The lithic technology is now more similar to the MSA I/Klasies River industry at KRM (Wurz, 2002). As the technology in SBLS differs and intact features such as hearths are well preserved, this layer likely belongs to a different member. The coastal ecology and lithic technology of SMONE are similar to those of the Mossel Bay lower phase in the Deacon sample. In contrast, BOS and SBLS correspond more to the coastal ecology for the MSA I phase in the Deacon sample (Langejans et al., 2017). The lithic technology of BOS, however, is similar to the MSA II/Mossel Bay lower and that of SBLS to the MSA I; indicating that coastal ecological changes did not occur synchronously with lithic technological approaches. Interestingly, the Tip Cross Sectional Area (TCSA) values for the points from SBLS are midway between the values for dart and javelin tip ranges, and the TCSA values for points in SMONE and BOS and MSA II, in general, are in the range for thrusting spears (Lombard, 2021). This may indicate a change in prey availability and capture methods in SBLS. Smaller lithics and prevalence of

bovid 1 processed elements may be linked to the trapping and snaring of smaller fauna that might have made an appearance during MIS 5, as suggested by [Dusseldorp and Langejans \(2015\)](#). The large mammal fauna from layers SMONE to SBLS signals intense occupation and resource extraction in this phase. The abundant small fauna, especially size 1 bovinds, have been burnt and have cutmarks. Furthermore, elements considered low-ranking, such as pelves and phalanges, show significantly more processing marks than other elements, perhaps indicating environmental stress ([Reynard, 2022b](#)).

The BOS-SBLS layers are broadly contemporaneous with PP 13B MIS 5d-e assemblages ([Brenner et al., 2022](#)) and with YFT 1 and HDP 1 on the west coast. The shellfish densities for PP 13B MIS d-e are very low, especially for the earliest evidence of shellfish exploitation at 164 ka (0.2 kg/m³). A changing coastal environment is also reflected during MIS 5c-e at PP 13B. Brown mussels are completely dominant in MIS 5e, and white mussels become much more prevalent in MIS 5d. The lithic artifacts at PP 13B also occur in low densities from MIS 5d-e, with especially the MIS 5e assemblage showing infrequent retouch and edge damage ([Thompson et al., 2010](#); [Brenner et al., 2022](#)). This may point to sporadic visits to the coast during this time period at PP 13B.

At HDP 1, episodic visits to the Atlantic west coast are also indicated during MIS 5d-e by the shellfish and lithic evidence. Granite limpets (*Cymbula granatina*) and black mussels (*Choromytilus meridionalis*) are dominant, and for stone tools, complete reduction sequences for local raw materials and importation of higher quality raw material tools are evident ([Will et al., 2013](#)). The consistency in the foraging and lithic behavior is interpreted as an indication of systematic coastal adaptation in MIS 5e ([Will et al., 2013](#); [Kyriacou et al., 2015](#)). These authors consider that the fast deposition rate that might be implied by the dates may indicate LSA intensity of shellfish exploitation ([Niespolo et al., 2021a, b](#), [Klein et al., 2004](#)). At YFT 1, limpets and black mussels are the most numerous taxa ([Klein et al., 2004](#); [Avery et al., 2008](#)) in the ca. 120–113 ka layers ([Niespolo et al., 2021a](#)). The lithic technology is very similar to that of HDP1 ([Wurz, 2012](#); [Will et al., 2013](#)). Although coastal exploitation was not as intensive as in the LSA ([Klein et al., 2004](#); [Avery et al., 2008](#)), stable adaptation to the coast with systematic foraging of shellfish occurred ([Tribolo et al., 2022](#)).

For the period between 100 and ca.130 ka, systematic exploitation of coastal resources occurred on the south and west coast of South Africa, but seemingly at various levels of intensity. Layer SMONE at KRM, older than 100 ka, showed the highest degree of residential occupation for the sites discussed in this study, whereas the other two layers, BOS and SBLS, and the PP 13B MIS 5c assemblage indicated somewhat lesser degrees of residential occupation. The visits to PP13B during MIS 5d-e, HDP1 and YFT 1 during MIS 5c-e show sporadic low-intensity occupation. However, these suppositions based on shellfish densities need to be interpreted with care and do not

necessarily relate to occupation intensity and shellfish exploitation patterns ([Jerardino, 2016a, b](#)). Herein, we have shown that the taphonomic alteration of shell midden deposits is an important factor that needs to be considered when discussing shellfish densities. Furthermore, occupational intensity is reflected by various measures ([Gravel-Miguel et al., 2022](#); [Reynard, 2022](#)), and the inferences made here need to be interpreted within this wider context.

KRM presents an extended sequence covering more than 70 ka, and most publications on the site discuss broad changes for the whole period on the basis of time-averaged data ([Langejans et al., 2012, 2017](#); [Reynard and Wurz 2020](#); [Reynard, 2022b](#) for recent examples of this). This is an important approach, but further progress in understanding landscape-wide changes and correlations is more likely when more specific information can be compared that involves limited time averaging ([Braun et al., 2021](#)). This is especially relevant for exploring pre-100 ka coastal adaptation. For KRM, it has been shown that fluctuations in shellfish exploitation patterns, coastal ecology, and lithic technology occur within a temporal window between just before 106 ka and after 110 ka. Capturing these changes would have been lost if the data were combined in a larger grouping, as is customary when time-averaged data are presented to investigate palaeo-environmental trends.

Although some models regard coastal environments as primary in the development of innovations and symbolic behaviors ([Marean, 2014](#); [Will et al., 2016](#)), innovations occur in other regions across the globe within this time period as well, sporadically at first, with a stronger signal that emerges at around 100 ka ([Wadley, 2021](#)). In South Africa, for example, crystals were collected at Ga-Mohana in the Kalahari basin at 105 ka ([Wilkins et al., 2021](#)), and on the Cape coast at Pinnacle Point, seashells may have been collected as beauty objects ([Jerardino and Marean, 2010](#)). Ochre-related innovations from the Cape coastal region occur at this time, for example, the possible heating of ochre at Pinnacle Point ([Watts, 2010](#)) and abalone shells with remnants of a compound ochre liquid from BBC ([Henshilwood et al., 2011](#)). It is the establishment of such innovations on a sub-continental scale and interaction between populations, coastal and inland, that is relevant to understanding cumulative cultural evolution and the human niche ([Kissel and Fuentes, 2018](#); [Meneganzin and Currie, 2022](#)). The layers discussed in this paper are older than 100 ka and contain limited evidence of ochre and other artifacts conventionally interpreted as symbolic and innovative.

6 Conclusion

One of the goals of this paper was to contextualize middening at KRM throughout the sequence to provide a more detailed framework for understanding coastal exploitation. Shell middens occur throughout the sequence at KRM in various stages of preservation. A wide range of post-depositional taphonomic processes, such as secondary carbonate formation,

compaction, soft-sediment deformation, and shell dissolution, impacted the preservation of shell-bearing deposits at KRM. The LSA middens contain well-preserved intact shells within highly porous layers, and the Howiesons Poort layers show variable post-depositional processes, with some samples, especially from the western area of Cave 2, showing abundant intact shell fragments. The MSA II/Mossel Bay lower shell middens are from a coarse context and cemented with secondary carbonate, and the internal porosity of some samples may be indicative of decalcification. The microstratigraphic sample from the SBLS contact in the Witness Baulk demonstrates conditions of high moisture and soft sediment deformation. The older MSA I shell middens from the base of the Witness Baulk contain more intact evidence for shell middens and secondary processes such as dumping. The microstratigraphic analysis underscores that shellfish density and visibility must be interpreted with care when inferring the degree of shellfish exploitation, as post-depositional processes significantly impact the preservation and chemical conditions of the shell.

A more precise temporal framework for the base of the MSA II shell-bearing deposits at KRM is provided. The MIS 5c-d MSA II deposits at KRM are, for the first time, precisely integrated into a window of time before 110 ka and after 106 ka based on U-Th dates on stalagmites. The dating relates to a hiatus after forming BOS, during which secondary carbonate formed on an exposed surface. The BOS layer, older than 110 ka, represents the base of the SASL sub-member, and SBLS likely falls within another member. The coastal environment in layer SMONE, younger than 106 ka, contained sheltered areas within a rocky coast. However, in BOS and especially in SBLS, dating to after 110 ka, the degree of shelteredness decreased. BOS and SBLS probably relate to a period with more rocky exposed shores. The lithic technology changed only in layer SBLS underlying BOS and is similar to the MSA I. The dated early Mossel Bay shell middens discussed in this study are broadly contemporaneous with those from YFT 1, HDP 1, and some of the PP 13B shell-bearing deposits and provide further evidence for the time period during which systematic coastal exploitation became more established on the South African coast.

Data availability statement

The raw data supporting the conclusion of this article will be made available by the authors without undue reservation.

Author contributions

SW is the principal investigator of the Klasies River main site, generated the data, co-analyzed the shellfish sample,

conceptualized the article, and co-wrote the paper. RP undertook the U-Th dating and co-wrote the paper. SMM conducted the micromorphological and geoarchaeological analysis and co-wrote the paper.

Funding

SW was funded by a National Research Foundation African Origins Platform grant (AOP no. 98826) and a DST-NRF Centre of Excellence in Palaeosciences Operational Support Grant (COEOP2020-20). Funding received by Robyn Pickering is from the NRF African Origins Platform (AOP150924142990) and DST-NRF Centre of Excellence in Palaeosciences Operational Support Grant (COE2018-10OP). Funding for instrumentation used in the analysis of the micromorphology samples was provided by a Deutsche Forschungsgemeinschaft grant to C. Miller (MI 1748/1-1). We are indebted to the Baden-Württemberg Stiftung for the financial support for the micromorphology component of this research project by the Elite programme for Postdocs (grant to SM).

Acknowledgments

We would like to thank the topic editor, Manuel Will, and the two reviewers, Erich Fisher and Ingrid Ward. U-Th dating was undertaken at the University of Melbourne, thanks to John Hellstrom, Helen Green, and Petra Bajo. The authors thank Kokeli Ryano for assisting with data on the shellfish and Silje Bentsen for aiding greatly in the sampling of the deposits. The authors thank Chris Miller for collecting two of the micromorphology blocks and Panos Kritikakis for the preparation of thin sections.

Conflict of interest

The authors declare that the research was conducted in the absence of any commercial or financial relationships that could be construed as a potential conflict of interest.

Publisher's note

All claims expressed in this article are solely those of the authors and do not necessarily represent those of their affiliated organizations or those of the publisher, the editors, and the reviewers. Any product that may be evaluated in this article, or claim that may be made by its manufacturer, is not guaranteed or endorsed by the publisher.

References

- Aldeias, V., and Bicho, N. (2016). Embedded behavior: Human activities and the construction of the mesolithic shellmound of cabeço da amoreira, muge, Portugal. *Geoarchaeology* 31 (6), 530–549. doi:10.1002/gea.21573
- Allsopp, N., Colville, J. F., and Verboom, G. A. (2014). *Fynbos: Ecology, evolution, and conservation of a megadiverse region*. Oxford: Oxford University Press.
- Andersen, S. H. (2000). 'Køkkenmøddinger' (Shell middens) in Denmark: A survey. *Proc. Prehist. Soc* 66, 361–384. doi:10.1017/S0079497X00001857
- Avery, G., Halkett, D., Orton, J., Steele, T., Tusenius, M., and Klein, R. (2008). The Ysterfontein 1 Middle Stone Age rock shelter and the evolution of coastal foraging. *S. Afr. Archaeol. Bull. Goodwin Ser.* 2008, 66–89.
- Bada, J. L., and Deems, L. (1975). Accuracy of dates beyond the 14C dating limit using the aspartic acid racemisation reaction. *Nature* 255 (5505), 218–219. doi:10.1038/255218a0
- Bar-Matthews, M., Marean, C. W., Jacobs, Z., Karkanas, P., Fisher, E. C., Herries, A. I., et al. (2010). A high resolution and continuous isotopic speleothem record of paleoclimate and paleoenvironment from 90 to 53 ka from Pinnacle Point on the south coast of South Africa. *Quat. Sci. Rev.* 29 (17–18), 2131–2145. doi:10.1016/j.quascirev.2010.05.009
- Bateman, M. D., Carr, A. S., Murray-Wallace, C. V., Roberts, D. L., and Holmes, P. J. (2008). A dating intercomparison study on Late Stone Age coastal midden deposits, South Africa. *Geoarchaeology* 23 (6), 715–741. doi:10.1002/gea.20243
- Binneman, J. N. F. (1995). Symbolic construction of communities during the Holocene later stone age in the southeastern Cape. Johannesburg: University of the Witwatersrand. [Phd thesis].
- Braun, D. R., Faith, J. T., Douglass, M. J., Davies, B., Power, M. J., Aldeias, V., et al. (2021). Ecosystem engineering in the quaternary of the west coast of South Africa. *Evol. Anthropol.* 30 (1), 50–62. doi:10.1002/evan.21886
- Braun, K., Bar-Matthews, M., Ayalon, A., Zilberman, T., and Matthews, A. (2017). Rainfall isotopic variability at the intersection between winter and summer rainfall regimes in coastal South Africa (Mossel Bay, Western Cape Province). *South Afr. J. Geol.* 120 (3), 323–340. doi:10.25131/jgssaj.120.3.323
- Brenner, M. J., Ryano, K. P., and Wurz, S. (2022). Coastal adaptation at Klasies River main site during MIS 5c-d (93, 000–110, 000 years ago) from a southern Cape perspective. *J. Isl. Coast. Archaeol.* 17 (2), 218–245. doi:10.1080/15564894.2020.1774444
- Brenner, M. J., and Wurz, S. (2019). A high-resolution perspective on MIS 5c-d lithic assemblages from Klasies River main site Cave 1. *J. Archaeol. Sci. Rep.* 26, 101891. doi:10.1016/j.jasrep.2019.101891
- Butzer, K. W. (1982). "Geomorphology and sediment stratigraphy," in *The middle stone age at Klasies River mouth in South Africa*. Editors R. Singer and J. Wymer (Chicago: Chicago University Press), 33–42.
- Canti, M. G. (2017). "Mollusc shell," in *Archaeological soil and sediment micromorphology*. Editors C. Nicosia and G. Stoops (Chichester: John Wiley & Sons), 43–46.
- Cawthra, H. C., Bergh, E. W., Wiles, E. A., and Compton, J. S. (2021). Late Quaternary deep marine sediment records off southern Africa. *South Afr. J. Geol.* 124 (4), 1007–1032. doi:10.25131/sajg.124.0059
- Chase, B. M., and Meadows, M. E. (2007). Late Quaternary dynamics of southern Africa's winter rainfall zone. *Earth. Sci. Rev.* 84 (3–4), 103–138. doi:10.1016/j.earscirev.2007.06.002
- Corrêa, G. R., Schaefer, C. E., and Gilkes, R. J. (2013). Phosphate location and reaction in an archaeoanthrosol on shell-mound in the lakes region, rio de Janeiro state, Brazil. *Quat. Int.* 315, 16–23. doi:10.1016/j.quaint.2013.09.036
- de Wet, W. M., and Compton, J. S. (2021). Bathymetry of the South African continental shelf. *Geo-Mar. Lett.* 41 (3), 40–19. doi:10.1007/s00367-021-00701-y
- Deacon, H. J., and Geleijnse, V. B. (1988). The stratigraphy and sedimentology of the main site sequence, Klasies River, South Africa. *South Afr. Archaeol. Bull.* 43 (147), 5–14. doi:10.2307/3887608
- Deacon, H. J. (1995). Two late Pleistocene-Holocene archaeological depositories from the southern Cape, South Africa. *South Afr. Archaeol. Bull.* 50, 121–131. doi:10.2307/3889061
- Deo, J. N., Stone, J. O., and Stein, J. K. (2004). Building confidence in shell: Variations in the marine radiocarbon reservoir correction for the northwest coast over the past 3, 000 years. *Am. Antiq.* 69 (4), 771–786. doi:10.2307/4128449
- Duarte, C., Iriarte, E., Diniz, M., and Arias, P. (2019). The microstratigraphic record of human activities and formation processes at the Mesolithic shell midden of Poças de São Bento (Sado Valley, Portugal). *Archaeol. Anthropol. Sci.* 11 (2), 483–509. doi:10.1007/s12520-017-0519-0
- Dupont, L. M., Zhao, X., Charles, C., Faith, J. T., and Braun, D. (2022). Continuous vegetation record of the greater Cape floristic region (south Africa) covering the past 300 000 years (IODP U1479). *Clim. Past.* 18 (1), 1–21. doi:10.5194/cp-18-1-2022
- Dusseldorp, G. L., and Langejans, G. H. J. (2013). Carry that weight: Coastal foraging and transport of marine resources during the South African middle stone age. *South Afr. Humanit* 25 (1), 105–135.
- Dusseldorp, G. L., and Langejans, G. H. (2015). *Trapping' the past? Hunting for remote capture techniques and planned coastal exploitation during MIS 5 at Blombos cave and Klasies River, South Africa*. Leiden: Analecta Praehist.
- Eggs, S. M., Grün, R., McCulloch, M. T., Pike, A. W., Chappell, J., Kinsley, L., et al. (2005). *In situ* U-series dating by laser-ablation multi-collector ICPMS: New prospects for quaternary geochronology. *Quat. Sci. Rev.* 24 (23–24), 2523–2538. doi:10.1016/j.quascirev.2005.07.006
- Engelbrecht, C. J., Landman, W. A., Engelbrecht, F. A., and Malherbe, J. (2015). A synoptic decomposition of rainfall over the Cape south coast of South Africa. *Clim. Dyn.* 44, 2589–2607. doi:10.1007/s00382-014-2230-5
- Faul, I. (2021). A palaeoecological and taphonomic analysis of microfossils from MIS 5 layers in Cave 1, Klasies River main site. South Africa: University of the Witwatersrand. Unpublished MSc dissertation.
- Feathers, J. K. (2002). Luminescence dating in less than ideal conditions: Case studies from Klasies River main site and duinefontein, south Africa. *J. Archaeol. Sci.* 29 (2), 177–194. doi:10.1006/jasc.2001.0685
- Fisher, E. C., Bar-Matthews, M., Jerardino, A., and Marean, C. W. (2010). Middle and Late Pleistocene paleoscape modeling along the southern coast of South Africa. *Quat. Sci. Rev.* 29 (11–12), 1382–1398. doi:10.1016/j.quascirev.2010.01.015
- Göden, M. (2014). *Geoarchäologische Untersuchungen zur Fundplatzgenese von Hoedjiespunt 1. Western Cape, Südafrika*: University of Tübingen. Unpublished MSc thesis.
- Goldberg, P., and Byrd, B. F. (1999). The interpretive potential of micromorphological analysis at prehistoric shell midden sites on Camp Pendleton. *Pac. Coast Archaeol. Soc. Q.* 35 (4), 1–23.
- Goldberg, P. (2000). Micromorphology and site formation at Die Kelders cave I, south Africa. *J. Hum. Evol.* 38 (1), 43–90. doi:10.1006/jhev.1999.0350
- Goldberg, P., Miller, C. E., Schiegl, S., Ligouis, B., Berna, F., Conard, N. J., et al. (2009). Bedding, hearths, and site maintenance in the Middle Stone age of Sibudu cave, KwaZulu-Natal, South Africa. *Archaeol. Anthropol. Sci.* 1 (2), 95–122.
- Gravel-Miguel, C., De Vynck, J., Wren, C. D., Murray, J. K., and Marean, C. W. (2022). Were prehistoric coastal sites more intensively occupied than inland sites? Using an agent-based model to understand the intensity of prehistoric coastal occupation, and what it means for studies on the evolution of the coastal adaptation. *Quat. Int.* 638–639, 148–158. doi:10.1016/j.quaint.2022.02.003
- Grün, R., Shackleton, N. J., and Deacon, H. J. (1990). Electron-spin-resonance dating of tooth enamel from Klasies River mouth cave. *Curr. Anthropol.* 31 (4), 427–432. doi:10.1086/203866
- Gutiérrez-Zugasti, I., Andersen, S. H., Araújo, A. C., Dupont, C., Milner, N., and Monge-Soares, A. M. (2011). Shell midden research in Atlantic Europe: State of the art, research problems and perspectives for the future. *Quat. Int.* 239 (1–2), 70–85. doi:10.1016/j.quaint.2011.02.031
- Hale, J. C., Benjamin, J., Woo, K., Astrup, P. M., McCarthy, J., Hale, N., et al. (2021). Submerged landscapes, marine transgression and underwater shell middens: Comparative analysis of site formation and taphonomy in Europe and North America. *Quat. Sci. Rev.* 258, 106867. doi:10.1016/j.quascirev.2021.106867
- Hellstrom, J., and Pickering, R. (2015). Recent advances and future prospects of the U-Th and U-Pb chronometers applicable to archaeology. *J. Archaeol. Sci.* 56, 32–40. doi:10.1016/j.jas.2015.02.032
- Hellstrom, J. (2003). Rapid and accurate U/Th dating using parallel ion-counting multi-collector ICP-MS. *J. Anal. At. Spectrom.* 18 (11), 1346–1351. doi:10.1039/b308781f
- Hellstrom, J. (2006). U-Th dating of speleothems with high initial 230Th using stratigraphical constraint. *Quat. Geochronol.* 1 (4), 289–295. doi:10.1016/j.quageo.2007.01.004
- Henshilwood, C. S., d'Errico, F., Van Niekerk, K. L., Coquinot, Y., Jacobs, Z., Lauritzen, S. E., et al. (2011). A 100, 000-year-old ochre-processing workshop at Blombos cave, south Africa. *Science* 334 (6053), 219–222. doi:10.1126/science.1211535
- Henshilwood, C. S., Sealy, J. C., Yates, R., Cruz-Urube, K., Goldberg, P., Grine, F. E., et al. (2001). Blombos cave, southern Cape, south Africa: Preliminary report on the 1992–1999 excavations of the middle stone age levels. *J. Archaeol. Sci.* 28 (4), 421–448. doi:10.1006/jasc.2000.0638

- Jacobs, Z. (2010). An OSL chronology for the sedimentary deposits from pinnacle point cave 13B—A punctuated presence. *J. Hum. Evol.* 59 (3-4), 289–305. doi:10.1016/j.jhevol.2010.07.010
- Jerardino, A., and Marean, C. W. (2010). Shellfish gathering, marine paleoecology and modern human behavior: Perspectives from cave PP13B, Pinnacle Point, South Africa. *J. Hum. Evol.* 59 (3-4), 412–424. doi:10.1016/j.jhevol.2010.07.003
- Jerardino, A., and Navarro, R. (2021). Pleistocene and Holocene procurement of the clam *Donax serra* (Bivalvia: Donacidae) along the southern Cape coast of South Africa. *J. Archaeol. Sci. Rep.* 38, 103062. doi:10.1016/j.jasrep.2021.103062
- Jerardino, A. (2016a). On the origins and significance of Pleistocene coastal resource use in southern Africa with particular reference to shellfish gathering. *J. Anthropol. Archaeol.* 41, 213–230. doi:10.1016/j.jaa.2016.01.001
- Jerardino, A. (2016b). Shell density as proxy for reconstructing prehistoric aquatic resource exploitation, perspectives from southern Africa. *J. Archaeol. Sci. Rep.* 6, 637–644. doi:10.1016/j.jasrep.2015.06.005
- Karkanas, P., Bar-Yosef, O., Goldberg, P., and Weiner, S. (2000). Diagenesis in prehistoric caves: The use of minerals that form *in situ* to assess the completeness of the archaeological record. *J. Archaeol. Sci.* 27 (10), 915–929. doi:10.1006/jasc.1999.0506
- Karkanas, P., Brown, K. S., Fisher, E. C., Jacobs, Z., and Marean, C. W. (2015). Interpreting human behavior from depositional rates and combustion features through the study of sedimentary microfossils at site Pinnacle Point 5-6, South Africa. *J. Hum. Evol.* 85, 1–21. doi:10.1016/j.jhevol.2015.04.006
- Kissel, M., and Fuentes, A. (2018). ‘Behavioral modernity’ as a process, not an event, in the human niche. *Time Mind* 11 (2), 163–183. doi:10.1080/1751696X.2018.1469230
- Klein, R. G., Avery, G., Cruz-Urbe, K., Halkett, D., Parkington, J. E., Steele, T., et al. (2004). The Ysterfontein 1 Middle Stone Age site, South Africa, and early human exploitation of coastal resources. *Proc. Natl. Acad. Sci. U. S. A.* 101 (16), 5708–5715. doi:10.1073/pnas.0400528101
- Klein, R. G., and Bird, D. W. (2016). Shellfishing and human evolution. *J. Anthropol. Archaeol.* 44, 198–205. doi:10.1016/j.jaa.2016.07.008
- Kristen, I., Fuhrmann, A., Thorpe, J., Röhl, U., Wilkes, H., and Oberhänsli, H. (2007). Hydrological changes in southern Africa over the last 200 Ka as recorded in lake sediments from the Tswaing impact crater. *South Afr. J. Geol.* 110 (2-3), 311–326. doi:10.2113/gssajg.110.2-3.311
- Kyriacou, K., Blackhurst, D. M., Parkington, J. E., and Marais, A. D. (2016). Marine and terrestrial foods as a source of brain-selective nutrients for early modern humans in the southwestern Cape, South Africa. *J. Hum. Evol.* 97, 86–96. doi:10.1016/j.jhevol.2016.04.009
- Kyriacou, K., Parkington, J. E., Will, M., Braun, D. R., and Conard, N. (2015). Middle and later stone age shellfish exploitation strategies and coastal foraging at hoedjiespunt and lynch point, saldanha Bay, south Africa. *J. Archaeol. Sci.* 57, 197–206. doi:10.1016/j.jas.2015.01.018
- Langejans, G. H., Dusseldorp, G. L., and Thackeray, J. F. (2017). Pleistocene molluscs from Klasies River (south Africa): Reconstructing the local coastal environment. *Quat. Int.* 427, 59–84. doi:10.1016/j.quaint.2016.01.013
- Langejans, G. H., van Niekerk, K. L., Dusseldorp, G. L., and Thackeray, J. F. (2012). Middle stone age shellfish exploitation: Potential indications for mass collecting and resource intensification at Blombos cave and Klasies River, south Africa. *Quat. Int.* 270, 80–94. doi:10.1016/j.quaint.2011.09.003
- Lap, A. (2020). Bones for thought: A taphonomic study of the faunal remains from early MIS 5 at Klasies River main site. Johannesburg: University of the Witwatersrand. MSc dissertation.
- Larbey, C., Mentzer, S. M., Ligouis, B., Wurz, S., and Jones, M. K. (2019). Cooked starchy food in hearths ca. 120 kya and 65 kya (MIS 5e and MIS 4) from Klasies River Cave, South Africa. *J. Hum. Evol.* 131, 210–227. doi:10.1016/j.jhevol.2019.03.015
- Linstädter, J., and Kehl, M. (2012). The Holocene archaeological sequence and sedimentological processes at Ifri Oudadane, NE Morocco. *J. Archaeol. Sci.* 39 (10), 3306–3323. doi:10.1016/j.jas.2012.05.025
- Loftus, E., Lee-Thorp, J., Leng, M., Marean, C., and Sealy, J. (2019). Seasonal scheduling of shellfish collection in the middle and later stone ages of southern Africa. *J. Hum. Evol.* 128, 1–16. doi:10.1016/j.jhevol.2018.12.009
- Lombard, M. (2021). Variation in hunting weaponry for more than 300,000 years: A tip cross-sectional area study of Middle Stone Age points from southern Africa. *Quat. Sci. Rev.* 264, 107021. doi:10.1016/j.quascirev.2021.107021
- Marean, C. W., Bar-Matthews, M., Fisher, E., Goldberg, P., Herries, A., Karkanas, P., et al. (2010). The stratigraphy of the middle stone age sediments at pinnacle point cave 13B (Mossel Bay, western Cape province, south Africa). *J. Hum. Evol.* 59 (3-4), 234–255. doi:10.1016/j.jhevol.2010.07.007
- Marean, C. W. (2010). Pinnacle Point Cave 13B (Western Cape Province, South Africa) in context: The Cape floral kingdom, shellfish, and modern human origins. *J. Hum. Evol.* 59 (3-4), 425–443. doi:10.1016/j.jhevol.2010.07.011
- Marean, C. W. (2014). The origins and significance of coastal resource use in Africa and Western Eurasia. *J. Hum. Evol.* 77, 17–40. doi:10.1016/j.jhevol.2014.02.025
- Marean, C. W. (2016). The transition to foraging for dense and predictable resources and its impact on the evolution of modern humans. *Phil. Trans. R. Soc. B* 371 (1698), 20150239. doi:10.1098/rstb.2015.0239
- McAdams, C., Morley, M. W., Fu, X., Kandyba, A. V., Dereviako, A. P., Nguyen, D. T., et al. (2022). Late Pleistocene shell midden microstratigraphy indicates a complex history of human-environment interactions in the uplands of North Vietnam. *Philos. Trans. R. Soc. Lond. B Biol. Sci.* 377 (1849), 20200493. doi:10.1098/rstb.2020.0493
- Meneganzin, A., and Currie, A. (2022). Behavioural modernity, investigative disintegration & Rubicon expectation. *Synthese* 200, 47. doi:10.1007/s11229-022-03491-7
- Miller, C. E., Berthold, C., Mentzer, S. M., Leach, P., Ligouis, B., Tribolo, C., et al. (2016). Site-formation processes at Elands Bay cave, south Africa. *South Afr. Humanit.* 29 (1), 69–128.
- Morrissey, P., Mentzer, S. M., and Wurz, S. (2022). A critical review of the stratigraphic context of the MSA I and II at Klasies River main site, south Africa. *J. Paleolit. Archaeol.* 5 (1), 5–47. doi:10.1007/s41982-022-00110-2
- Nami, H. G., de la Peña, P., Vásquez, C. A., Feathers, J., and Wurz, S. (2016). Palaeomagnetic results and new dates of sedimentary deposits from Klasies River Cave 1, South Africa. *S. Afr. J. Sci.* 112 (11-12), 12. doi:10.17159/sajs.2016/20160051
- Niespolo, E. M., Sharp, W. D., Avery, G., and Dawson, T. E. (2021a). Early, intensive marine resource exploitation by Middle Stone Age humans at Ysterfontein 1 rockshelter, South Africa. *Proc. Natl. Acad. Sci. U. S. A.* 118 (16), e2020042118. doi:10.1073/pnas.2020042118
- Niespolo, E. M., Sharp, W. D., Avery, G., and Dawson, T. E. (2021b). Reply to Klein: Ysterfontein 1 shell midden (South Africa) and the antiquity of coastal adaptation. *Proc. Natl. Acad. Sci. U. S. A.* 118 (31), e2108794118. doi:10.1073/pnas.2108794118
- Oertle, A., Szabó, K., Gaqa, S., Cawthra, H. C., Esteban, I., Pargeter, J., et al. (2022). Peering into the unseen: Novel methods in identifying shell taxa from archaeological micro-fragments. *J. Archaeol. Sci.* 147, 105667. doi:10.1016/j.jas.2022.105667
- Parkington, J., Cunneane, S. C., and Stewart, K. M. (2010). “Coastal diet, encephalization, and innovative behaviors in the late Middle Stone Age of southern Africa,” in *Human brain evolution: The influence of freshwater and marine food resources* (New Jersey: Wiley & Blackwell), 189–202.
- Partridge, T. C., Demenocal, P. B., Lorentz, S. A., Paiker, M. J., and Vogel, J. C. (2013). Orbital forcing of climate over South Africa: A 200,000-year rainfall record from the pretoria saltpan. *Quat. Sci. Rev.* 16 (10), 1125–1133. doi:10.1016/S0277-3791(97)00005-X
- Pickering, R., Hancox, P. J., Lee-Thorp, J. A., Grün, R., Mortimer, G. E., McCulloch, M., et al. (2007). Stratigraphy, U-Th chronology, and paleoenvironments at gladysvale cave: Insights into the climatic control of South African hominin-bearing cave deposits. *J. Hum. Evol.* 53, 602–619. doi:10.1016/j.jhevol.2007.02.005
- Quick, L. J., Meadows, M. E., Bateman, M. B., Kirsten, K. L., Mäusbacher, R., Haberzettl, T., et al. (2016). Vegetation and climate dynamics during the last glacial period in the fynbos-afrotemperate forest ecotone, southern Cape, South Africa. *Quat. Int.* 404, 136–149. doi:10.1016/j.quaint.2015.08.027
- Reynard, J. P. (2022b). Occupations and ecology at Klasies River from MIS 5-3: Preliminary taphonomic analyses of faunal remains from the Deacon and Wurz excavations. *Frontiers*.
- Reynard, J. P. (2022). Tracking occupational intensity using archaeological data: case studies from the late pleistocene in the southern cape of South Africa. *J. Archaeol. Method Theory* 29, 214–250. doi:10.1007/s10816-021-09513-x
- Reynard, J. P., and Wurz, S. (2020). The palaeoecology of Klasies River, South Africa: An analysis of the large mammal remains from the 1984–1995 excavations of Cave 1 and 1A. *Quat. Sci. Rev.* 237, 106301. doi:10.1016/j.quascirev.2020.106301
- Sealy, J., and Galimberti, M. (2011). “Shellfishing and the interpretation of shellfish sizes in the Middle and Later Stone Ages of South Africa,” in *Trekking the shore: Changing coastlines and the antiquity of coastal settlement*. Editors N. F. Bicho, J. A. Haws, and L. G. Davis (New York: Springer), 405–419.
- Sherwood, J., Barbetti, M., Ditchburn, R., Kimber, R. W. L., McCabe, W., Murray-Wallace, C. V., et al. (1994). A comparative study of Quaternary dating techniques

- applied to sedimentary deposits in southwest Victoria, Australia. *Quat. Sci. Rev.* 13 (2), 95–110. doi:10.1016/0277-3791(94)90035-3
- Simon, M. H., Ziegler, M., Barker, S., van der Meer, M. T., Schouten, S., and Hall, I. R. (2020). A late Pleistocene dataset of Agulhas Current variability. *Sci. Data* 7, 385–412. doi:10.1038/s41597-020-00689-7
- Simon, M. H., Ziegler, M., Bosmans, J., Barker, S., Reason, C. J. C., and Hall, I. R. (2015). Eastern South African hydroclimate over the past 270,000 years. *Sci. Rep.* 5, 18153. doi:10.1038/srep18153
- Singer, R., and Wymer, J. (1982). *The middle stone age at Klasies River mouth in South Africa*. Chicago: University of Chicago Press.
- Steele, T. E., and Klein, R. G. (2008). Intertidal shellfish use during the middle and later stone age of South Africa. *Archaeofauna* 17 (6), 63–76.
- Stein, J. K. (2008). “Geoarchaeology and archaeostratigraphy view from a northwest coast shell midden,” in *Case studies in environmental archaeology* (New York, NY: Springer), 61–80.
- Stein, J. K. (1982). Geologic analysis of the Green River shell middens. *Southeast. Archaeol.* 22, 39.
- Stein, J. K., Green, D., and Sherwood, S. (2011). “Sediment analysis,” in *Is it a house? Archaeological excavations at English camp, san juan island* (Washington/Seattle: University of Washington Press), 45–63.
- Stein, J. K. (1992). The analysis of shell middens. *Deciphering a shell midden* 1, 24.
- Stoops, G. (2003). *Guidelines for analysis and description of soil and regolith thin sections*. Madison, Wisconsin: Soil Science Society of America.
- Taylor, V. K., Barton, R. N. E., Bell, M., Bouzouggar, A., Collcutt, S., Black, S., et al. (2011). The Epipalaeolithic (Iberomaurusian) at Grotte des Pigeons (Tafoualt), Morocco: a preliminary study of the land Mollusca. *Quat. Int.* 244 (1), 5–14. doi:10.1016/j.quaint.2011.04.041
- Thackeray, J. F. (1988). Molluscan fauna from Klasies River, south Africa. *South Afr. Archaeol. Bull.* 43 (147), 27–32. doi:10.2307/3887610
- Thompson, E., Williams, H. M., and Minichillo, T. (2010). Middle and late Pleistocene Middle Stone Age lithic technology from Pinnacle Point 13B (Mossel Bay, Western Cape Province, South Africa). *J. Hum. Evol.* 59 (3–4), 358–377. doi:10.1016/j.jhevol.2010.07.009
- Tribolo, C., Mercier, N., Martin, L., Taffin, N., Miller, C. E., Will, M., et al. (2022). Luminescence dating estimates for the coastal MSA sequence of Hoedjiespunt 1 (South Africa). *J. Archaeol. Sci. Rep.* 41, 103320. doi:10.1016/j.jasrep.2021.103320
- Van Andel, T. H. (1989). Late Pleistocene sea levels and the human exploitation of the shore and shelf of southern South Africa. *J. Field Archaeol.* 16 (2), 133–155. doi:10.2307/529887
- van Wijk, Y., Tusenius, M. L., Rust, R., Cowling, R. M., and Wurz, S. (2017). Modern vegetation at the Klasies River archaeological sites, Tsitsikamma coast, south-eastern Cape, south Africa: A reference collection. *Plant Ecol. Evol.* 150 (1), 13–34. doi:10.5091/plevevo.2017.1286
- Vanara, N., and Maire, R. (2006). Genesis of phototropic biospeleothems in Guizhou (China): Occurrence of biocorrosion, microphantomization and algal precipitation. *Geol. Belg.* 9, 337–347.
- Viles, H. A. (1984). Biokarst: Review and prospect. *Prog. Phys. Geogr. Earth Environ.* 8, 523–542. doi:10.1177/030913338400800403
- Villagran, X. S., Balbo, A. L., Madella, M., Vila, A., and Estevez, J. (2011a). Experimental micromorphology in tierra del fuego (Argentina): Building a reference collection for the study of shell middens in cold climates. *J. Archaeol. Sci.* 38 (3), 588–604. doi:10.1016/j.jas.2010.10.013
- Villagran, X. S., Balbo, A. L., Madella, M., Vila, A., and Estevez, J. (2011b). Stratigraphic and spatial variability in shell middens: Microfacies identification at the ethnohistoric site tunel VII (tierra del fuego, Argentina). *Archaeol. Anthropol. Sci.* 3 (4), 357–378. doi:10.1007/s12520-011-0074-z
- Villagran, X. S. (2014). Experimental micromorphology on burnt shells of *Anomalocardia brasiliana* (Gmelin 1791) (Bivalvia, Veneridae) and its potential for identification of combustion features on shell-matrix sites. *Geoarchaeology* 29 (5), 389–396. doi:10.1002/geoa.21486
- Villagran, X. S., Flores, C., Olgún, L., Rebolledo, S., Durán, V., Sandoval, C., et al. (2021). “Microstratigraphy and faunal records from a shell midden on the hyperarid coast of the Atacama Desert (Taltal, Chile),” in *South American contributions to world archaeology* (Cham: Springer), 249–281.
- Villagran, X. S., Huisman, D. J., Mentzer, S. M., Miller, C. E., and Jans, M. M. (2017). “Bone and other skeletal tissues (pp. 11–38),” in *Archaeological soil and sediment micromorphology*. Editors C. Nicosia and G. Stoops (Chichester: John Wiley & Sons).
- Villagran, X. S., and Poch, R. M. (2014). A new form of needle-fiber calcite produced by physical weathering of shells. *Geoderma* 213, 173–177. doi:10.1016/j.geoderma.2013.08.015
- Villagran, X. S. (2019). The shell midden conundrum: Comparative micromorphology of shell-matrix sites from South America. *J. Archaeol. Method Theory* 26 (1), 344–395. doi:10.1007/s10816-018-9374-2
- Vogel, J. C., Tobias, P. V., Raath, M. A., Maggi-Cecchi, J., and Doyle, G. A. (2001). “Radiometric dates for the middle Stone age in South Africa,” in *Humanity from african naissance to coming millennia-colloquia in human biology and palaeoanthropology* (Johannesburg: Wits University Press), 261–268.
- Voigt, E. A. (1973b). Klasies River Mouth: An exercise in shell analysis. *Bul. Transvaal Mus.* 14, 14–15.
- Voigt, E. A. (1973a). Stone age molluscan utilization at Klasies River mouth caves. *S. Afr. J. Sci.* 69, 306–309.
- Voigt, E. A. (1982). “The molluscan fauna,” in *The middle stone age at Klasies River mouth in South Africa*. Editors R. Singer and J. Wymer (Chicago: University of Chicago Press), 155–186.
- Wadley, L. (2015). Those marvellous millennia: The middle stone age of southern Africa. *Azania Archaeol. Res. Afr.* 50 (2), 155–226. doi:10.1080/0067270X.2015.1039236
- Wadley, L. (2021). What stimulated rapid, cumulative innovation after 100,000 years ago? *J. Archaeol. Method Theory* 28 (1), 120–141. doi:10.1007/s10816-020-09499-y
- Ward, I., Moe-Astrup, P., and Merigot, K. (2019). At the water’s edge: Micromorphological and quantitative mineral analysis of a submerged Mesolithic shell midden at Hjarnø Sund, Denmark. *J. Archaeol. Sci.* 102, 11–25. doi:10.1016/j.jas.2018.12.009
- Watts, I. (2010). The pigments from pinnacle point cave 13B, Western Cape, South Africa. *J. Hum. Evol.* 59 (3–4), 392–411. doi:10.1016/j.jhevol.2010.07.006
- Wilkins, J., Schoville, B. J., Pickering, R., Gliganic, L., Collins, B., Brown, K. S., et al. (2021). Innovative *Homo sapiens* behaviours 105,000 years ago in a wetter Kalahari. *Nature* 592 (7853), 248–252. doi:10.1038/s41586-021-03419-0
- Will, M., Kandel, A. W., and Conard, N. J. (2019). Midden or Molehill: The role of coastal adaptations in human evolution and dispersal. *J. World Prehist.* 32 (1), 33–72. doi:10.1007/s10963-018-09127-4
- Will, M., Kandel, A. W., Kyriacou, K., and Conard, N. J. (2016). An evolutionary perspective on coastal adaptations by modern humans during the Middle Stone Age of Africa. *Quat. Int.* 404, 68–86. doi:10.1016/j.quaint.2015.10.021
- Will, M., Parkington, J. E., Kandel, A. W., and Conard, N. J. (2013). Coastal adaptations and the middle stone age lithic assemblages from hoedjiespunt 1 in the Western Cape, south Africa. *J. Hum. Evol.* 64 (6), 518–537. doi:10.1016/j.jhevol.2013.02.012
- Wurz, S., Bentsen, S. E., Reynard, J., Van Pletzen-Vos, L., Brenner, M., Mentzer, S., et al. (2018). Connections, culture and environments around 100,000 years ago at Klasies River main site. *Quat. Int.* 495, 102–115. doi:10.1016/j.quaint.2018.03.039
- Wurz, S. (2021). Technocomplexes and chronostratigraphy for MIS 6–1 in southern Africa. *South Afr. J. Geol.* 124 (4), 1083–1092. doi:10.25131/sajg.124.0058
- Wurz, S. (2002). Variability in the middle stone age lithic sequence, 115,000–60,000 years ago at Klasies River, south Africa. *J. Archaeol. Sci.* 29 (9), 1001–1015. doi:10.1006/jasc.2001.0799
- Wurz, S. (2012). The significance of MIS 5 shell middens on the cape coast - a lithic perspective from Klasies River and Ysterfontein 1. *Quat. Int.* 270, 61–69.
- Yoshioka, S., and Kitano, Y. (1985). Transformation of aragonite to calcite through heating. *Geochem. J.* 19 (4), 245–249. doi:10.2343/geochemj.19.245